Title

The 26S Proteasome Utilizes a Kinetic Gateway to Prioritize Substrate Degradation

Journal

Cell, 177(2)

ISSN

0092-8674

Authors

Bard, Jared AM
Bashore, Charlene
Dong, Ken C
et al.

Publication Date

2019-04-01

DOI

10.1016/j.cell.2019.02.031

Peer reviewed

HHS Public Access

Author manuscript

Cell. Author manuscript; available in PMC 2020 April 04.

Published in final edited form as:

Cell. 2019 April 04; 177(2): 286–298.e15. doi:10.1016/j.cell.2019.02.031.

The 26S Proteasome utilizes a kinetic gateway to prioritize substrate degradation

Jared A.M. Bard[1,2,4], **Charlene Bashore**[1,2,5], **Ken C. Dong**[1,2,3], and **Andreas Martin**[1,2,3,6,*]

[1]Department of Molecular and Cell Biology, University of California at Berkeley, Berkeley, California 94720, USA

[2]California Institute for Quantitative Biosciences, University of California at Berkeley, Berkeley, California 94720, USA

[3]Howard Hughes Medical Institute, University of California at Berkeley, Berkeley, California 94720, USA

[4]Present address: Department of Biochemistry & Molecular Biology, The University of Chicago, Chicago, Illinois 60637, USA

[5]Present address: Genentech, Inc., 1 DNA Way, South San Francisco, California 94080, USA

[6]Lead Contact

Summary

The 26S proteasome is the principal macromolecular machine responsible for protein degradation in eukaryotes. However, little is known about the detailed kinetics and coordination of the underlying substrate-processing steps of the proteasome, and their correlation with observed conformational states. Here, we used reconstituted 26S proteasomes with unnatural amino acid-attached fluorophores in a series of FRET and anisotropy-based assays to probe substrate-proteasome interactions, the individual steps of the processing pathway, and the conformational state of the proteasome itself. We develop a complete kinetic picture of proteasomal degradation, which reveals that the engagement steps prior to substrate commitment are fast relative to subsequent deubiquitination, translocation and unfolding. Furthermore, we find that non-ideal substrates are rapidly rejected by the proteasome, which thus employs a kinetic proofreading mechanism to ensure degradation fidelity and substrate prioritization.

Graphical Abstract

*Correspondence: a.martin@berkeley.edu.

Author contributions: J.A.M.B. and A.M. designed experiments, J.A.M.B. performed biochemical experiments, C.B. helped with experimental design, and K.C.D. assisted with the preparation of materials. All authors contributed to manuscript preparation.

Declaration of Interests: The authors declare no competing interests.

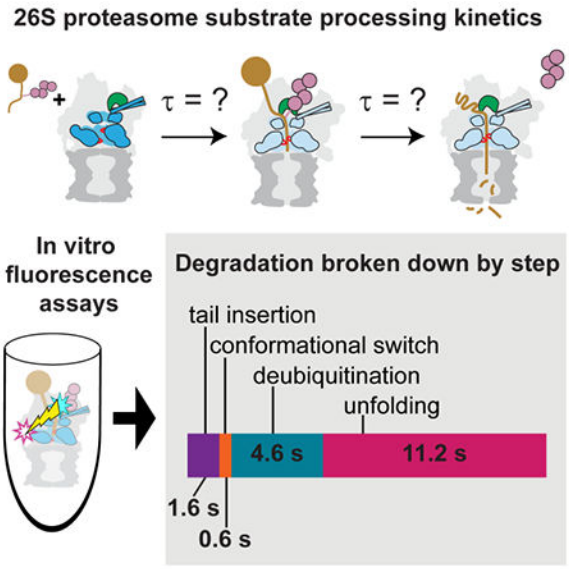

In Brief

A complete kinetic picture of proteasomal degradation reveals that the engagement steps prior to substrate commitment are fast relative to subsequent deubiquitination, translocation and unfolding

Keywords

26S proteasome; ubiquitin-proteasome system; AAA+ protease; ATP-dependent protein degradation; unnatural amino-acid incorporation

Introduction:

Specific protein degradation is essential for quality control, homeostasis, and the regulation of diverse cellular processes, such as the cell cycle and stress response (Chen et al., 2011; Hershko and Ciechanover, 1998). In eukaryotic cells, this degradation is primarily catalyzed by the 26S proteasome, which recognizes, unfolds, and degrades proteins that have been modified with lysine-attached poly-ubiquitin chains (Bard et al., 2018). To accomplish its dual roles in quality control and signaling, the proteasome must be able to degrade certain proteins consistently and under tight kinetic constraints, while maintaining a high promiscuity necessary to process thousands of polypeptides with diverse characteristics, yet avoiding unregulated proteolysis of cellular proteins in general. This precise regulation is accomplished by the proteasome's complex molecular architecture and a bipartite degradation signal for substrate recognition that consists of suitable poly-ubiquitin modifications and an unstructured initiation region of appropriate length and sequence composition (Fishbain et al., 2015; Fishbain et al., 2011; Inobe et al., 2011; Peth et al., 2010; Prakash et al., 2004; Takeuchi et al., 2007).

Based on available structural and biochemical information, we can infer the processing steps necessary for substrate degradation, which include the binding of ubiquitin to a proteasomal

receptor, insertion of the unstructured initiation region into the central processing pore, the removal of ubiquitin chains, and the unfolding and translocation of the polypeptide into the 20S core particle for proteolysis. Substrate access to the sequestered proteolytic active sites is controlled by the 19S regulatory particle that caps one or both ends of the 20S core (Groll et al., 2000), and can be further divided into the base and lid subcomplexes with 9 subunits each (Glickman et al., 1998). The base contains multiple ubiquitin receptors and a ring-shaped AAA+ (ATPases Associated with diverse cellular Activities) motor formed by the six distinct ATPases Rpt1-Rpt6, whose ATP binding and hydrolysis drives translocation and unfolding of substrates (Deveraux et al., 1994; Elsasser et al., 2004; Husnjak et al., 2008; Shi et al., 2016; van Nocker et al., 1996). After ubiquitin binding, a substrate's flexible initiation region likely must reach through the rigid N-ring formed by the OB-fold domains of Rpt1-Rpt6, before engaging with conserved pore loops of the ATPase domains that translate the energy of ATP hydrolysis into mechanical pulling (Beckwith et al., 2013; Erales et al., 2012). The lid subcomplex is bound to one side of the base and contains the deubiquitinating enzyme Rpn11 (Lander et al., 2012; Pathare et al., 2014; Verma et al., 2002; Worden et al., 2014; Yao and Cohen, 2002).

Both *in vivo* and *in vitro* structural studies revealed that the 26S proteasome adopts multiple conformations, which can be divided into a substrate-free apo (s1) state and substrate-processing (s3-like) states (Albert et al., 2017; Asano et al., 2015; Beck et al., 2012; Lander et al., 2012; Matyskiela et al., 2013; Sledz et al., 2013; Unverdorben et al., 2014; Wehmer et al., 2017). While the s1 state is the primary conformation adopted by the ATP-bound proteasome in the absence of protein substrate, the s3-like state appears more conducive to processive degradation and can be stabilized by stalling a substrate during translocation (de la Pena et al., 2018; Dong et al., 2018; Guo et al., 2018). In this degradation-competent s3-like state, the central channel of the motor aligns with the N-ring and the entrance to the 20S core, and the ATPase ring is more planar with uniform interfaces between neighboring Rpt subunits (Matyskiela et al., 2013). Upon transition from the s1 to s3 states, the lid rotates relative to the base, placing Rpn11 directly above the central channel where it removes ubiquitin chains *en bloc* from substrates as they are translocated into the motor (Worden et al., 2017; Worden et al., 2014). Similar s3-like states have also been observed by incubating the proteasome with nucleotide analogs such as ATPγS (Sledz et al., 2013).

Despite this wealth of structural information, it remains elusive what induces the proteasome to switch from the s1 to the s3-like states, and how these distinct conformations are coordinated with the substrate-processing pathway. Furthermore, little is known about the relative timing and coordination of individual degradation steps, which limits our understanding of how the proteasome determines the turnover kinetics for particular substrates, how it can establish general protein homeostasis, and what step is rate limiting. Finally, numerous substrates have been observed to resist degradation by the proteasome, but the mechanisms underlying this discrimination are still unclear (Fishbain et al., 2015; Fishbain et al., 2011; Inobe et al., 2011; Peth et al., 2010; Prakash et al., 2004; Takeuchi et al., 2007; Yu et al., 2016).

Here we reveal the complete kinetic picture of substrate processing by the 26S proteasome. We designed a series of fluorescence- and FRET-based assays to specifically measure the

kinetics of individual degradation steps in a fully reconstituted and thus well-controlled system, without contamination by additional regulatory proteins such as the deubiquitinase Ubp6 (Hu et al., 2005). These novel tools allowed us to track the interactions between a substrate's initiation region and the AAA+ motor, the conformational changes of the proteasome, substrate deubiquitination by Rpn11, and cleavage into peptides. Our results reveal the rate-limiting step of degradation, identify the trigger for the proteasome's conformational switch from the si to the s3 state, and elucidate the regulation of Rpn11's deubiquitination activity. Furthermore, we analyzed the degradation effects of varying substrate characteristics, including the stability of the folded domain, the number of ubiquitin chains, and the length and composition of the unstructured initiation region, offering new insights into how the proteasome selects and prioritizes its substrates in a complex cellular environment.

Results:

Unnatural amino-acid labeling of the proteasome

To deconvolute individual steps of substrate degradation and track the coupled conformational changes of the proteasome, we sought to develop Forster resonance energy transfer (FRET)-based assays sensitive to specific processing events. One requirement for these assays was the ability to site-specifically attach fluorophores to the 19S regulatory particle with minimal perturbations. We thus devised a method for the incorporation and labeling of 4-azido-L-phneylalanine (AzF) in *Saccharomyces cerevisiae* base and lid sub-complexes using previously established heterologous expression systems (Fig. 1A) (Amiram et al., 2015; Bard and Martin, 2018; Beckwith et al., 2013; Chatterjee et al., 2013; Chin et al., 2002; Lander et al., 2012). To increase the labeling specificity, solvent-exposed cysteines were reversibly protected before reacting the incorporated AzF with a dibenzocyclooctyne-linked fluorophore (van Geel et al., 2012), leading to 50-80% labeling efficiency with minimal off-target reactions (Fig. 1A). Proteasomes reconstituted with these fluorescently labeled base and lid sub-complexes exhibited full activity in substrate degradation (Fig. 1B, Fig. S1A).

Tracking the Conformational State of the Proteasome

Published cryo-EM structures of the 26S proteasome revealed major conformational changes between the substrate-free and substrate-processing states, yet it remains unclear how these transitions are coupled to specific degradation steps. We identified the lid subunit Rpn9 and the N-terminal coiled-coil of the base subunits Rpt4 and Rpt5 as promising positions for the placement of a donor-acceptor pair to directly monitor the proteasome conformational dynamics through FRET (Fig. 1C). As the lid rotates relative to the base during the transition to a substrate-engaged state, the distance between Rpn9 and the N-terminal helix of Rpt5 decreases by almost 40 A, and we predicted that the FRET efficiency for fluorophores at these positions would increase accordingly.

Proteasomes were thus reconstituted using lid with donor-labeled Rpn9-S111AzF and base with acceptor-labeled Rpt5-Q49AzF, and bulk FRET efficiencies were measured under steady-state conditions (Fig. 1D). Incubation with the non-hydrolyzable nucleotide analog

ATPγS has previously been shown to induce the substrate engaged-like s3 state (Sledz et al., 2013), and it correspondingly caused a significant increase in FRET compared to proteasome in ATP (Fig. 1D). Interaction with ubiquitin-bound Ubp6 has also been found to shift the conformational equilibrium towards the substrate-engaged state (Aufderheide et al., 2015; Bashore et al., 2015), which was confirmed by our assay showing an increase in FRET efficiency when catalytically inactive Ubp6 was added together with tetra-ubiquitin. There was no change in FRET, however, upon addition of 100 μM unanchored ubiquitin chains. Despite binding to proteasomal receptors, as indicated by their inhibition of substrate degradation (Fig. S1B), these unanchored chains hence do not induce a conformational change of the proteasome.

We then measured the FRET signal of actively degrading proteasomes and observed an increase similar to that of proteasomes trapped in the s3 state by ATPγS. The signal increased further upon addition of ubiquitinated substrate in the presence of 1,10-phenanthroline (*o*PA), an inhibitor of the deubiquitinating enzyme Rpn11 (Verma et al., 2002). Preventing Rpn11-mediated deubiquitination inhibits degradation by stalling substrate translocation through the central channel, most likely when the attached ubiquitin chain reaches the narrow entrance to the N-ring pore, thus trapping and synchronizing proteasomes in a substrate engaged state (Worden et al., 2017). We conclude that actively processing proteasomes spend most of the time in an s3-like conformation.

Rapid substrate engagement induces the proteasome conformational switch

While the steady-state FRET-based assay confirmed that actively degrading proteasomes switch away from the s1 state, it provided no information about when this switch occurs. To determine the relationship between the conformational change and specific processing steps, and to gain insight into the overall coordination of substrate degradation, we developed a series of fluorescence-based assays for measuring detailed kinetics (Fig. 2).

Our model substrate, titin-I27^{V15P}-23-K-35, was constructed from a titin-I27 domain containing the destabilizing V15P mutation and a C-terminal unstructured region with a single lysine for ubiquitin-chain attachment in a defined position, leaving a 35-residue ‘tail’ for proteasome engagement (Fig. S1C) (Bashore et al., 2015; Saeki et al., 2005). The time required for degradation of this substrate was determined by tracking the anisotropy of a fluorophore attached to the N-terminus of the titin folded domain (Bhattacharyya et al., 2016). Gel-based assays confirmed the rapid degradation into peptides (Fig. 2B), and Michaelis-Menten analyses established the substrate affinity (K_M = 0.22 μM) and degradation rate (kcat = 2.34 sub enz^{-1} min^{-1}) under multiple-turnover, steady-state conditions (Fig. S1D). In subsequent single-turnover degradation experiments with saturating concentrations of proteasome, we observed an initial fast increase in anisotropy, followed by a second increase and an exponential signal decay (Fig. 2C, Fig. S2A, Table S3). The observed two-step increase in signal is characteristic of multiple sequential kinetic processes. When the substrate was mixed with proteasomes containing the catalytically dead Rpn11^{AXA} mutant, the anisotropy signal also rapidly increased, but did neither show the second increase nor the exponential decay (Fig. S2A). Mixing with ATPγS-bound wild-type proteasomes led to no change in signal at all (Fig. 2C). The initial anisotropy increase is thus

likely a result of ATP hydrolysis-dependent substrate engagement by the AAA+ motor, whereas the second, deubiquitination-dependent increase may report on the reduced substrate flexibility upon ubiquitin-chain removal and pulling of the folded domain against the motor entrance. The signal decay then reflects the mechanical unfolding, translocation, and cleavage of the substrate into small peptides. This decay (and all kinetic traces later measured for individual substrate-processing steps) fit best to a double exponential curve, consisting of a dominant fast phase and a low-amplitude slow phase. Since the slow-phase likely originates from a small population of partially aggregated or incompletely ubiquitinated substrate, we focused our analyses on the fast phase, as done in previous studies (Beckwith et al., 2013; Worden et al., 2017). Combining the time constant for the exponential decay in anisotropy (τ = 11 s) and the delay associated with the initial increase (to = 7 s) reveals that complete degradation of our titin model substrate occurs with a time constant of 18 s. The first step of substrate processing after ubiquitin binding requires the insertion of the unstructured initiation region into the pore of the proteasomal motor (Peth et al., 2010). We specifically tracked the kinetics of this tail-insertion process using a FRET-based assay that relied on the energy transfer between a donor fluorophore placed near the central channel of the motor, in the linker between the N-domain and the ATPase domain of Rpt1 (Rtp1-I191AzF), and an acceptor fluorophore attached to the substrate's initiation tail (Fig. 2D, Table S4). To kinetically isolate tail-insertion from subsequent steps of substrate processing, we treated the proteasome with *o*PA, thereby preventing progression past the ubiquitin-modified lysine and trapping the proteasome with the inserted substrate in a high-FRET state. After stopped-flow mixing of acceptor-labeled substrate and donor-labeled, *o*PA-treated proteasome, we observed a rapid increase in FRET, as indicated by the quenching of donor fluorescence and the reciprocal increase in acceptor fluorescence (Fig. S2B), revealing a time constant of 1.6 s (Fig. 2D). Since ubiquitin binding to the proteasome was found to occur significantly faster, with $\tau \sim 0.4$ s based on previous single-molecule measurements (Lu et al., 2015), we can conclude that the 1.6 s time constant is largely determined by substrate-tail insertion after ubiquitin interaction with a proteasomal receptor. Tail insertion thus occurred on a similar time scale as the change in anisotropy seen upon substrate mixing with Rpn11^{AXA}-containing proteasome (Fig. S2C). We confirmed that the fluorophore on the unstructured initiation region had no major effects on the degradation rate (Table S3), and no signal change was observed when mixing proteasome with substrate lacking a ubiquitin chain (Fig. 2D). Tail insertion was also prevented in the ATPγS-induced s3 state of the proteasome (Fig. 2D), in which the centrally positioned Rpn11 potentially obstructs access to the central pore.

We next measured the kinetics of conformational switching after substrate addition to Rpn11-inhibited proteasomes, using the above-mentioned FRET-based assay that tracks the relative distance between the base and lid sub-complexes (Fig. 2E, Table S5). Because binding of unanchored ubiquitin chains alone had no effect on the conformational state of the proteasome, we hypothesized that engagement of the substrate's unstructured region with the pore loops of the AAA+ motor is required to trigger the switch. Indeed, upon mixing proteasome with substrate, the acceptor fluorescence increased with a time constant of 2.2 s, closely tracking with the tail insertion event. A reciprocal signal change was observed in the donor channel, confirming the underlying FRET (Fig. S2D). Examination of

early time points revealed that the FRET signal for substrate tail insertion increased immediately after mixing, whereas the signal for the conformational switch showed a 0.4 s delay (Fig. 2F). The delay indicates that the substrate tail is inserted first. Subsequent interactions with the motor pore-loops then lead to a rapid switch of the proteasome from the si to a substrate-engaged, s3-like state. This model is supported by our previous studies showing that the pore-loops of Rpt subunits at the top of the sl-state spiral staircase are particularly important for degradation, as they may make first contact with a substrate (Beckwith et al., 2013).

After substrate engagement, the proteasome must remove attached ubiquitin chains before proceeding to unfold and translocate the rest of the polypeptide. Therefore, a final FRET-based assay was designed to selectively monitor the deubiquitination event, this time by tracking the energy transfer between donor-labeled ubiquitin and an acceptor fluorophore attached to the substrate adjacent to the ubiquitinated lysine. Co-translocational ubiquitin removal from the substrate caused a loss in acceptor fluorescence, while pre-incubation of proteasomes with ATPγS abolished the signal change (Fig. 2G, Fig. S2E). Stopped-flow measurements of the FRET signal upon mixing substrate with saturating amounts of wild-type proteasome in the presence of ATP revealed that deubiquitination occurs with a total time constant of 6.8 s (Table S6), which reflects the sum of the time required for binding, tail insertion, and deubiquitination. This time constant also encompasses ubiquitin-chain release from the proteasome (which is expected to occur in less than 0.5 s, see below) or the time for translocation of the substrate polypeptide beyond the zone of FRET (which happens with a rate of at least 15 AA s^{-1}, see below). Mixing of the substrate with $Rpn11^{AXA}$-containing proteasome led to a more than 2-fold lower signal change that is likely caused by a change in fluorophore environment when ubiquitin binds to the catalytically-dead Rpn11 (Fig. S2F).

By comparing the various time constants described above, we can derive the first complete kinetic model of proteasomal substrate processing and estimate the time required for each step following substrate binding (Fig. 2H). Initial tail insertion proceeds with a time constant of 1.6 s, followed by a rapid conformational switch after 0.4 s. The removal of the ubiquitin chain then happens within ~ 5 s, and mechanical substrate unfolding, translocation, and cleavage take an additional 11 s.

The proteasome can quickly remove multiple ubiquitin chains, but is slowed down by stable domains

Our kinetic characterization revealed that most of the substrate processing time is spent on deubiquitination and unfolding or translocation. To further probe the relative contributions of these steps to overall degradation time, we modified our model substrate, either by changing the stability of the folded domain (Fig. 3A,B, Fig. S3) or by increasing the number of ubiquitin chains that need to be removed during degradation (Fig. 3C, Fig. S4).

The experiments shown in Fig. 2 were performed with titin-$I27^{V15P}$-23-K-35, which has a thermodynamic stability of DG = −19 kJ mol^{-1} (Fig. S3). Based on previously reported mutants of titin-I27 (Kenniston et al., 2003), we constructed and measured the degradation of a further destabilized variant, titin-$I27^{V13P/V15P}$-23-K-35 (DG = −8 kJ mol^{-1}), as well as the wild-type version, titin-I27-23-K-35 (DG = −24 kJ mol^{-1}). As seen for other substrates

(Johnston et al., 1995; Kraut et al., 2012; Peth et al., 2013), increasing the stability of the folded titin domain significantly increased the overall time required for degradation. Analysis by SDS-PAGE showed that the most stable titin variant is rapidly deubiquitinated and then slowly unfolded and degraded (Fig. 3B). Hence, the unfolding event itself is the rate-limiting step of degradation for this substrate, which remains stably engaged after ubiquitin-chain removal and while the proteasome attempts to overcome the tough unfolding barrier. The less stable titin variants exhibited no accumulation of the deubiquitinated species on the proteasome, indicating that unfolding and deubiquitination occur on similar time scales for these substrates. Interestingly, the stability of the titin variants correlated with their ability to stimulate proteasomal ATP hydrolysis. The most stable substrate (titin-I27-23-K-35) showed the strongest stimulatory effect (Table S7), most likely because its slow unfolding caused the proteasome to spend the least time in the non-stimulated, substrate-free state during degradation under saturating conditions. The least stable titin-$I27^{V13P/15P}$ variant was degraded with a total time constant of 15 s. Considering that all initial processing steps, including deubiquitination, take 6.8 seconds, and assuming rapid subsequent unfolding of the destabilized titin domain, we can estimate a minimum translocation rate of 15 AA s^{-1} for the 116 amino acids that remain to be threaded after unfolding.

To test the effects of additional ubiquitin chains on substrate degradation, we added a second or third lysine into the unstructured tail of our model substrate. The modification of all three lysine was confirmed by SDS-PAGE after ubiquitination with methyl-ubiquitin (Fig. S4A,B) or by trimming poly-ubiquitin chains with the deubiquitinase AMSH (Fig. S4C), which does not remove the substrate-attached ubiquitin moiety (Michel et al., 2015). Michaelis-Menten analyses showed that substrates with one, two, or three ubiquitin chains have similar binding affinities and degradation rates (Fig. S1). Importantly, all three substrates also showed no difference in degradation rate under single-turnover conditions (Fig. 3C), suggesting that while the removal of the first ubiquitin chain takes 5 seconds, subsequent chains must be removed much more quickly. One model for this change in deubiquitination rate comes from our previous findings that the rate-limiting step of isopeptide cleavage by Rpn11 is a ubiquitin-induced conformational switch of its Insert-1 region (Worden et al., 2017). We propose that after Rpn11 removes the first ubiquitin chain, it does not immediately switch back to the inactive conformation, but is poised to bind and promote fast cleavage of nearby ubiquitin chains that rapidly approach Rpn11 as the substrate is translocated into the central pore.

Substrates with poor initiation regions fail to engage with the proteasome

It has been established that substrates with short (< 25 residues) or low-complexity initiation regions are not efficiently degraded *in vitro* and have extended *in vivo* half-lives (Fishbain et al., 2015; Fishbain et al., 2011; Inobe et al., 2011; Prakash et al., 2004; Yu et al., 2016). To investigate this phenomenon, we modified the initiation region of our model substrate by varying the length of the terminal tail following the single ubiquitinated lysine or by replacing it with a low complexity, serine-rich sequence previously shown to severely impair degradation (Fishbain et al., 2011; Yu et al., 2016). Tracking proteasomal processing by SDS-PAGE revealed that substrates with a 35 or 25 AA tail were completely degraded into

peptides, whereas the truncated tail variants with 11 or 1 AA were primarily deubiquitinated and released (Fig 4A, Fig. S5). Deubiquitination and release of the short-tail substrates could be monitored by the decrease in anisotropy, albeit with a smaller amplitude than for complete proteolysis into peptides (Fig. S6A,B). Using this anisotropy readout in multiple-turnover titrations revealed that the short tails cause significant K_M defects for titin-I27^{V15P}-23-K-11 (K_M = 1.2 μM) and titin-I27^{V15P}-23-K-1 (K_M = 2.7 μM), compared to titin-I27^{V15P}-23-K-35 (K_M = 0.2 μM) (Fig. S1, Fig. S6D,E).

We then analyzed the kinetics of tail insertion through increase of FRET between donor labeled, Rpn11-inhibited proteasome and acceptor-labeled substrate, as in Fig. 2D (Fig. 4B, Table 1). Shorter tails appeared to enter the central pore more rapidly, yet their FRET amplitude was severely reduced, with 11 and 1 AA tails showing only 25% and 16%, respectively, of the signal change detected for the 35-residue tail. These low amplitudes are most likely a consequence of the truncated tails being too short to reach from the narrow N-ring entrance to the pore loops, thus preventing a stable engagement with the AAA+ motor. After initial rapid insertion, these tails may quickly escape again from the central channel, which is consistent with the observed increase in the apparent rate constants for short tail insertion, k_{app}, that reflects the sum of both, on and off rates (Table 1). The elevated off rates lead to an increase in K_M for the processing of short-tailed substrates under multiple-turnover conditions, even though their ubiquitin targeting signal is unchanged (Fig. S6E). Based on the affinity for the 1-AA tail variant (K_m = 2.7 μM) and the previously determined on-rate for ubiquitin binding to the proteasome (8.5 10^5 M^{1} s^{-1}, (Lu et al., 2015), we can approximate $k_{of} \sim 2.3\ s^{-1}$ for the dissociation of tailless substrates or unanchored ubiquitin chains after Rpn11 cleavage.

Though short tails insert, at least briefly, into the pore of the motor, we found that substrates with those truncated initiation regions fail to trigger the conformational change of the proteasome (Fig. 4C). In contrast to the small amplitude and fast kinetics we observed for the tail-insertion traces, the conformational change traces for truncated tails exhibited almost no amplitude, supporting our model that interactions between the substrate polypeptide and the motor's pore loops drive the switch in proteasome conformation. These data also confirm our results presented in Fig. 1D that binding of unanchored ubiquitin chains to proteasomal receptors does not induce the conformational change.

Despite their failure to engage and trigger proteasome conformational switching, shorttailed substrates are slowly deubiquitinated (Fig. 4A). The loss of anisotropy during the multiple-turnover processing of the 1 AA tail substrate (Fig. S6E) reveals a time constant of 45 s for this engagement-independent deubiquitination, which is significantly slower than the 6.8 s observed for translocation-coupled deubiquitination of the long-tailed substrate (Fig. 2G). The almost 7-fold difference in deubiquitination rate agrees well with the previously revealed acceleration of Rpn11-mediated ubiquitin cleavage by mechanical substrate translocation into the AAA+ motor (Worden et al., 2017). Since short-tailed substrates fail to induce the conformational switch of the proteasome, their slow deubiquitination likely occurs while the proteasome is in the s1 state or during brief, spontaneous sampling of s3-like conformation.

Like the short tails, the low complexity serine-rich tail also led to a significant KM defect in multiple-turnover processing and exhibited a decreased FRET amplitude for tail insertion (Fig. S6E, Fig. 4B). In contrast to the short tails, however, it also showed slower tail-insertion kinetics, with a kapp four times lower than that of a complex tail of the same length. Thus, in addition to having an elevated ratio of koff/kon (and therefore KM), the on-rate of the serine-rich tail is decreased. The conformational change induced by this substrate was also slow and of a low magnitude, with the defects again being amplified compared to those measured in tail insertion. Both the tail-insertion and conformational change assays rely on a stalled state, with the substrate's initiation region stably engaged by the AAA+ motor. The small FRET-signal amplitudes for the serine-rich tail thus indicate a rapid substrate escape from the proteasome pore and a consequent low probability of commitment, explaining the observed slow degradation and frequent release (Fig. 4A). Low-complexity regions thus hinder substrate processing in several ways: by slowing the onset of tail insertion, inhibiting the conformational change, and likely by reducing the motor grip required for unfolding and translocation.

How are proteasomes *in vivo* able to rapidly turn over high priority substrates, such as cell-cycle regulators, while ubiquitinated proteins with poor initiation regions and therefore slow processing kinetics compete for proteasomal ubiquitin receptors? To test this scenario *in vitro*, we performed competition experiments, in which the degradation of a fluorescently labeled, ubiquitinated titin-I27^{V15P}-23-K-35 substrate was tracked in the presence of unlabeled ubiquitinated substrates with varying tail architectures (Fig. 4D). While the unlabeled titin-I27^{V15P}-23-K-35 effectively inhibited degradation of its labeled counterpart, substrates with short or serine-rich initiation regions were poor competitors, even at concentrations above their measured KM values. Conversely, the long-tailed substrate effectively prevented the slow deubiquitination of substrates with poor initiation regions (Fig. S6C). These results can be explained by the high off rates and poor engagement of short or low-complexity tails with the ATPase motor. Their inability to compete also suggests that the ubiquitin-chain interactions with receptors on the proteasome is short lived. In contrast to these 'poor' substrates that do not prevent the proteasome from degrading other targets, non-degradable substrates such as amyloid-like fibers have been shown to recruit and stall proteasomes (Bauerlein et al., 2017), likely by efficiently engaging with the AAA+ motor but then resisting mechanical unfolding.

Substrates with ubiquitin-obstructed initiation regions depend on additional ubiquitin chains for degradation

The titin-I27^{V15P}-23-K-11 substrate described above contains a 11 AA tail C-terminal to the lysine-attached ubiquitin chain, and slow deubiquitination during proteasomal processing creates a 35-residue unstructured region that would otherwise be sufficient for processive degradation. Nevertheless, this substrate largely escapes degradation, likely because the flexible initiation region is not stably engaged with the AAA+ motor when the single, affinity-conferring ubiquitin chain is removed. In contrast to this model substrate, many proteins in the cell are modified with multiple ubiquitin chains, which has been shown to increase substrate affinity for the proteasome (Lu et al., 2015; Shabek et al., 2012). We therefore wondered whether the translocation-independent removal of ubiquitin chains

obstructing flexible initiation regions could enable complete substrate degradation, provided that an additional ubiquitin modification maintains the substrate's affinity for the proteasome during subsequent engagement. We tested this hypothesis by using SDS-PAGE to compare the proteasomal processing of an obstructed, short-tailed titin-I27^{V15P}-43-K-11 substrate with that of its double-lysine variant, titin-I27^{V15P}-23-K-19-K-11, containing an extra site for ubiquitin modification (Fig. 5). The presence of the second ubiquitin chain decreased the K_M from 2 μM to 1 μM (Fig. S6E), which is in contrast to the long-tailed substrates whose proteasome affinity is already high with a single ubiquitin chain and changes only minimally upon attachment of additional chains (Fig. S1D). Adding a second ubiquitin chain on the short-tailed substrate did not increase the velocity of processing, as titin-I27^{V15P}-43-K-11 and titin-I27^{V15P}-23-K-19-K-11 showed similar time constants (if_{ast} = 46 s ± 13 s) for the disappearance of ubiquitinated species (Table S8). For both substrates, slow, translocation-independent ubiquitin removal by Rpn11 appears to be rate-limiting and the first step of substrate processing. However, while titin-I27^{V15P}-43-K-11 was primarily deubiquitinated and released from the proteasome, titin-I27^{V15P}-23-K-19-K-11 was mostly degraded, as indicated by considerably stronger formation of peptide products and less accumulation of deubiquitinated protein (Fig. 5). These findings suggest that slow deubiquitination can make substrates with ubiquitin-obstructed initiation regions accessible for degradation, if additional ubiquitin chains keep the substrates associated with the proteasome. Accessory factors that modify the ubiquitination state of proteasome-bound substrates, such as Ubp6 and Hul5, may further act in concert with the proteasome's intrinsic mechanisms described here (Crosas et al., 2006).

Discussion

An intricate system of recognition and processing steps allows the 26S proteasome to select only appropriate substrates that contain both the correct ubiquitin-targeting signal and an unstructured initiation region, while maintaining the high promiscuity necessary to degrade hundreds of cellular proteins with diverse characteristics. Using FRET-based assays to measure the kinetics of individual substrate-processing events, we found that insertion and engagement of the unstructured initiation tail is fast, whereas most of the degradation time is spent on mechanical unfolding and translocation. We show that the proteasome rapidly transitions from the si state to a substrate-processing, s3-like state immediately after tail insertion, suggesting that substrate interactions with the pore loops of the AAA+ motor drive this global conformational switch. Premature transition to this state, however, prevents tail insertion and engagement, which highlights the importance of this intricate coordination between substrate processing steps and conformational switching of the proteasome.

We identified mechanical unfolding as the rate-determining step for degradation of our model proteins. Consistent with previous studies, we found that increasing the thermodynamic stability of a substrate's structured domain extends the time required for degradation. This analysis of unfolding rates for domain variants with three different stabilities provides a benchmark against which much of the proteome can be compared. Upstream of the proteasome, protein unfoldases like Cdc48/p97 could destabilize folded domains of proteins before they are targeted to the proteasome and thus increase their rate of degradation (Blythe et al., 2017; Bodnar and Rapoport, 2017; Olszewski et al., 2019). In

contrast to the thermodynamic stability, the presence of additional ubiquitin chains on already efficiently degraded substrates had no effect on the overall degradation rate. We propose that after the first ubiquitin-cleavage, which takes about 5 s, subsequent deubiquitination events can be significantly accelerated, because Rpn11 remains in its active state at least long enough to remove closely spaced ubiquitin chains from a translocating polypeptide. Other studies have shown that multiple ubiquitin chains can confer additional affinity for the proteasome (Lu et al., 2015; Shabek et al., 2012). Given our finding that removing extra chains does not affect the overall rate of degradation, it is not surprising that high-priority substrates, such as those ubiquitinated by the APC, contain multiple, closely spaced ubiquitin modifications (Kirkpatrick et al., 2006; Rape et al., 2006).

When investigating the requirements for substrate recognition and engagement, we found that ubiquitinated proteins with initiation regions of insufficient length or complexity were slowly deubiquitinated and released, rather than degraded, which explains previous findings of poor *in vitro* degradation or extended *in vivo* half-lives for those substrates (Fishbain et al., 2015; Peth et al., 2010). Interestingly, even substrates for which deubiquitination would reveal a sufficiently long initiation region escaped degradation, unless an additional ubiquitin chain maintained proteasome affinity to allow substrate engagement prior to release. Besides accelerating the degradation of stable proteins, unfoldases such as Cdc48/p97 may thus also play a critical role in preparing substrates for degradation by exposing unstructured initiation regions for efficient proteasomal engagement (Blythe et al., 2017; Bodnar and Rapoport, 2017; Olszewski et al., 2019). Short or low-complexity initiation regions rapidly enter the central channel of the proteasome, but cannot stably engage with the AAA+ pore loops and quickly escape again, leading to a significant increase of the substrate's K_M. Unlike the difference in K_M commonly observed for different ubiquitin modifications, this change is due to an increase in the substrate's off rate after the initial ubiquitin interaction. The kinetics of interactions between ubiquitin and its receptors, and between the initiation region and the motor thus represent alternative levers that can be used to tune the affinity of a substrate for the proteasome.

We propose that the initial ubiquitin-binding and tail-insertion events represent a dynamic gateway that is characterized by both, fast on and off rates, and controls the selection of appropriate substrates for proteasomal degradation (Fig. 6). If a substrate has the necessary requirements for processing, then tail engagement with the AAA+ motor reduces the off rate and induces the proteasome conformational switch that commits the substrate to unfolding, translocation-coupled deubiquitination, and degradation. As a consequence of this rapid ubiquitin sampling by the proteasome, binding of poor substrates does not considerably inhibit the degradation of higher-priority substrates with proper initiation regions, as seen in our *in vitro* competition experiments with short and long tailed proteins. This mechanism is similar to the kinetic proofreading mechanism used by the ribosome to recognize cognate amino acyl-tRNAs, in which rapid initial binding interactions are followed by an irreversible committed step (Rodnina and Wintermeyer, 2001). Our studies thus provide exciting new insights into how the proteasome prioritizes its substrates in the cell and coordinates its processing steps and conformational changes to ensure efficient protein degradation.

STAR Methods

CONTACT FOR REAGENT AND RESOURCE SHARING

Further information and requests for resources and reagents should be directed to and will be fulfilled by the Lead Contact, Andreas Martin (a.martin@berkeley.edu).

EXPERIMENTAL MODEL AND SUBJECT DETAILS

All proteins, except for the 20S core particle, were expressed in *Escherichia coli* using T7 expression vectors. The genes for all yeast proteins were cloned from *Saccharomyces cerevisiae* strain S288C. Usp2 and SENP2 are derived from *H. sapiens*, AMSH and Uba1 from *M. musculus*, sortase A from *S. aureus*, and all other genes are artificial. The Bl21-star(DE3) or Rosetta2(DE3)pLysS *E. coli* strains were used for protein expression as indicated for each protein. Cultures were grown in 2.5 L Ultra-Yield flasks (Thomson Instrument Company Cat#931136-B) shaking at 180 rpm at 37 °C. Induction times and temperatures are noted for individual proteins.

The 20S core particle was purified from the *S. cerevisiae* strain yAM54 (see below). Cultures were grown in YPD (Yeast extract, Peptone, and Dextrose) in 2.5 L Ultra-Yield flasks at 30 °C for 2 - 3 days harvested by resuspension in lysis buffer (see below) and popcorned into liquid nitrogen.

Name	Description	Genotype
yAM54	Pre1-3xFLAG	MATa his3Δ200, leu2-3,112 lys2-801 trp1Δ63 ura3-52 PRE1-3xFLAG::KANMX

METHOD DETAILS

Protein Purification—All plasmids used for purification are described in the key resources table. Additional information on the substrate amino acid sequences is available in Table S1.

After the final size-exclusion step all proteins were concentrated in Amicon Ultra spin concentrators, aliquoted, flash frozen in liquid N_2 and stored at −80 °C.

Except where noted, the concentrations of all proteins were determined by the absorbance at 280 nm.

Purification of 20S core: *S. cerevisiae* 20S core was purified from the Pre1-3xFLAG yeast strain yAM54 as previously described (Matyskiela et al., 2013). Briefly, yAM54 yeast were lysed under liquid nitrogen using a 6875 Freezer Mill Dual Chamber Cryogenic grinder (SPEX Sample Prep) and resuspended in lysis buffer (60 mM HEPES, pH 7.6, 500 mM NaCl, 1 mM EDTA, 0.2% NP-40). 20S core was immobilized on M2 anti-FLAG resin (Sigma), washed with buffer containing 1 M NaCl to remove bound regulatory particle, eluted from the resin using 3xFLAG peptide, and further purified by size-exclusion chromatography with a Superose 6 Increase 10/300 column (GE) equilibrated in GF buffer

(30 mM HEPES, pH 7.6, 50 mM NaCl, 50 mM KCl, 10 mM $MgCl_2$, 5% glycerol) with 0.5 mM TCEP.

Purification of wild-type base: Recombinant yeast base was purified after heterologous expression in *E. coli* using a slight modification of previously published methods (Beckwith et al., 2013). *E. coli* BL21-star(DE3) (Invitrogen) was co-transformed with the plasmids pAM81, pAM82, and pAM83 (derived from pETDuet, pCOLADuet, and pACYCDuet, respectively), coding for Rpt1 - Rpt6, Rpn1, Rpn2, Rpn13, the four base-assembly chaperones Rpn14, Hsm3, Nas2, and Nas6, and rare tRNAs. Bacteria were grown in 3 L of terrific broth (Novagen) to an OD_{600} = 0.8, then induced with 0.5 mM IPTG at 30 °C for 5 hours, followed by an overnight induction at 16 °C. The cells were pelleted and resuspended in NiA buffer (60 mM HEPES, pH 7.6, 100 mM NaCl, 100 mM KCl, 10 mM $MgCl_2$, 5% glycerol, and 20 mM imidazole) supplemented with 2 mg ml^{-1} lysozyme, benzonase (Novagen), and protease inhibitors (aprotinin, pepstatin, leupeptin and PMSF). Cells were lysed by sonication, the lysate was clarified by centrifugation for 30 minutes at 30,000 g, and the base subcomplex was purified by a three-step procedure, with 0.5 mM ATP present in all buffers. First, the His-Rpt3 containing complexes were purified using a 5 mL HisTrap FF crude (GE), then fully assembled complexes containing Flag-Rpt1 were selected for by using anti-Flag M2 affinity resin (Sigma), and finally, the complex was further purified using size-exclusion chromatography with a Superose 6 increase 10/300 column equilibrated in GF buffer with 1 mM ATP and 0.5 mM TCEP. The concentration of base was determined by Bradford assay using bovine serum albumin (BSA, Sigma) as a standard.

Purification and labeling of AzF-base: The base sub-complex containing 4-azido-L-phenylalanine (AzF) was expressed, purified, and labeled using a similar procedure with the following modifications (Bard and Martin, 2018). In addition to pAM81, pAM83, and an amber-codon containing variant of pAM82, a fourth plasmid (pAM87) containing the AzF tRNA synthetase/tRNA pair was used to co-transform Bl21-star(DE3) *E. coli.* This plasmid was constructed by replacing the IPTG-inducible synthetase in the pULTRA-CNF construct designed by the Schultz lab with the AzFRS.2.t1 synthetase evolved by the Isaacs lab (Amiram et al., 2015; Chatterjee et al., 2013). The pEvol-pAzFRS.2.t1 was a gift from Farren Isaacs (Addgene plasmid # 73546) and the pULTRA-CNF was a gift from Peter Schultz (Addgene plasmid # 48215). The cells were grown in 3 L of dYT media to an OD_{600} = 0.6, then pelleted, and resuspended in 0.5 L of terrific broth (Novagen) with added 2mM AzF (Amatek Chemical). The cells were shaken for 30 minutes at 30 °C to allow for uptake of the AzF, followed by induction with 0.5 mM IPTG for 5 hours at 30 °C and then 16 °C overnight. Purification followed the same protocol as for AzF-free base, except that after elution from the anti-Flag resin, the base was incubated with 150 gM 5,5'-dithiobis-(2-nitrobenzoic acid) (DTNB) for 10 minutes at room temperature to temporarily block any exposed cysteines. The base was then cooled back down to 4 °C and labeled overnight with 300 gM dibenzocyclooctyne (DBCO) conjugated fluorophore (Click Chemistry Tools). The reaction was quenched using 1 mM free AzF, followed by 2 mM dithiothreitol (DTT), and labeled base was then purified using size-exclusion chromatography as described above. Labeling efficiencies were estimated by comparing the absorbance-based concentration of fluorophore with the base concentration calculated by the Bradford assay.

Purification of lid: Recombinant yeast lid was also purified using a three-step procedure. The plasmids pAM80, pAM85, and pAM86, coding for Rpn3, Rpn5 - Rpn9, Rpn11, Rpn12, Sem1, and rare tRNAs, were modified from previously published plasmids to replace the affinity tags(Lander et al., 2012). Human rhinovirus (HRV) 3C protease-cleavable maltose binding protein was inserted at the N-terminus of Rpn6, and the N-terminus of Rpn12 was modified with a HRV-cleavable 6xHis tag. *E. coli* BL21-star(DE3) was co-transformed with these plasmids and then grown, induced, and lysed as described above for the base. The fully assembled lid was purified using a HisTrap and amylose resin (NEB), cleaved with HRV-protease, and purified on a Superose 6 Increase size-exclusion column equilibrated in GF buffer with 0.5 mM TCEP. Unnatural amino acid-containing lid was expressed and purified in a fashion similar to AzF-containing base, using the same DTNB blocking and DBCO-fluorophore labeling procedures after elution from the amylose resin. The HRV cleavage and overnight labeling were performed simultaneously, followed by quenching and size-exclusion chromatography.

Purification of substrates: All substrates were purified using the IMPACT system (NEB). The substrate was inserted into a T7-inducible plasmid derived from pET28a (Novagen) upstream of the intein and chitin binding domain (CBD) taken from pTXB1 (NEB). *E. coli* BL21-star(DE3) was transformed with this plasmid, grown in 3 L of dYT to an OD_{600} = 0.6, and induced with 0.5 mM IPTG for 3 hours at 30 °C. The cells were then resuspended in chitin buffer (60 mM HEPES, pH 7.6, 150 mM NaCl, 1 mM EDTA, 5% glycerol) with protease inhibitors (AEBSF, aprotinin, leupeptin, and pepstatin), and benzonase. Following lysis and clarification, the cells were bound in batch to 10 mL of chitin resin (NEB) for 1 hour at 4 °C, which was then washed with 100 mL of chitin buffer supplemented with an additional 500 mM NaCl, 0.2% Triton X-100, and protease inhibitors. The substrate was cleaved from the column by overnight incubation at 4 °C in a buffer containing 60 mM HEPES, pH 8.5, 150 mM NaCl, 1 mM EDTA, 5% glycerol, and 50 mM DTT. The substrate was collected from the column, run over 3 mL of fresh chitin resin to remove any uncleaved substrate, and then purified on a S75 16/60 size-exclusion chromatography column (GE) in GF buffer with 0.5 mM TCEP.

Purification of sortase A, Ubp6^{C188A}, SENP2, and Usp2: The proteins sortaseA, Ubc6^{C188A}, SENP2 and Usp2 were all purified using the same procedure. Plasmids containing the proteins were transformed into BL21-star(DE3) *E. coli*, which was grown in 2 L of terrific broth until OD_{600} = 0.6. Protein production was induced with 0.5 mM IPTG, the cells were incubated overnight at 18 °C, and were harvested in NiA buffer with benzonase, lysozyme and protease inhibitors. After lysis by sonication and clarification by centrifugation at 30,000g for 30 minutes, the protein was purified using a HisTrap and size-exclusion chromatography on a Superose 75 16/60 column (sortase A, SENP2, Usp2) or a Superdex 200 16/60 column (Ubp6^{C188A}) equilibrated in GF buffer. The plasmid used to express Usp2 was a gift from Cheryl Arrowsmith (Addgene plasmid # 36894). The plasmid used to express SENP2 protease was a gift from Guy Salvesen (Addgene plasmid # 16357) (Mikolajczyk et al., 2007). The plasmid used to express sortase A was a gift from Hidde Ploegh (Theile et al., 2013).

Labeling of substrates: Fluorophores were covalently attached to a single engineered cysteine in the substrate by maleimide chemistry. While there are two additional cysteines in the titin-I27 domain used, they are not solvent exposed. Substrates were dialyzed for 3 hours at room temperature into labeling buffer (30mM HEPES 7.2, 150 mM NaCl, 1 mM EDTA) using Slide-a-Lyzer mini dialysis cups (ThermoFisher), diluted to 100 μM and then incubated for 1 hour at room temperature with 200 μM fluorophore. Excess dye was then quenched with 1 mM DTT, and removed by size-exclusion chromatography on a Superdex 75 10/300 column equilibrated with GF buffer.

Where noted, the N-terminus of the substrate was labeled by sortase A (SrtA)-mediated ligation of a peptide (Theile et al., 2013). For the sortase modification, peptide (HHHHHHLPETGG) was purchased with 5-FAM conjugated to its N-terminus (Biomatik), and then ligated to 100 μM substrate using 20 μM recombinant 6xHis-SrtA in GF buffer supplemented with 1 mM DTT, 10 mM $CaCl_2$, and 0.5 mM peptide. For dual-labeled substrates, the sortase labeling was performed immediately following the fluorophore conjugation, before the excess dye was removed. The labeled substrate was selected for by binding to a 1 mL HisTrap HP (GE), followed by size-exclusion chromatography on a Superdex 75 10/300 column (GE) equilibrated with GF buffer.

The concentration of substrate was determined by quantifying the absorbance of the attached fluorophore (5-FAM = 492 nm, Cy5 = 646 nm). The substrates used in Figure 5 were prepared in a similar fashion, but using 5-FAM-LPETGG and without the HisTrap enrichment step. The concentration was calculated assuming a labeling efficiency of 80%.

Purification of Ubiquitin: Ubiquitin was expressed and purified as described previously (Worden et al., 2014). Briefly, Rosetta2 (DE3) pLysS *E. coli* cells were transformed with an IPTG-inducible expression plasmid (pET28a) containing *S. cerevisiae* ubiquitin. The cells were grown in terrific broth at 37 °C until the OD_{600} = 1.5-2.0 and ubiquitin expression was induced with 0.5 mM IPTG overnight at 18 °C. After expression, the cells were resuspended in lysis buffer (50 mM Tris-HCl, pH 7.6) containing 2 mg/mL lysozyme, benzonase, and protease inhibitors (aprotinin, pepstatin, leupeptin and PMSF). The cells were lysed by sonication, clarified by centrifugation, and contaminating proteins were precipitated by the addition of 60% perchloric acid to a final concentration of 0.5%. The soluble fraction containing ubiquitin was dialyzed overnight into 50 mM Na-acetate, pH 4.5, and purified by cation exchange on a 5 mL HiTrap SP FF column (GE) using a gradient of 0 - 0.5 M NaCl in 50 mM Na-acetate, pH 4.5. Peak fractions were concentrated and stored in ubiquitin storage buffer (20 mM Tris-HCl, pH 7.6, and 150 mM NaCl) at −80 °C.

Purification and labeling of ubiquitin: In order to label ubiquitin, a variant was expressed with an N-terminal cysteine inserted before the first methionine (MC-ubiquitin). This variant was expressed and purified as described previously (Worden et al., 2017). Briefly, Rosetta2 (DE3) pLysS *E. coli* cells were transformed with an IPTG-inducible expression plasmid (pET28a) containing MC-ubiquitin. The cells were grown in terrific broth (Novagen) at 37 °C until the OD_{600} = 1.5, and ubiquitin expression was induced with 0.5 mM IPTG overnight at 18 °C. After expression, the cells were resuspended in lysis buffer (50 mM Tris-HCl, pH 7.6) containing 2 mg mL^{-1} lysozyme, benzonase, and protease inhibitors

(aprotinin, pepstatin, leupeptin and PMSF). The cells were lysed by sonication, and contaminating proteins were precipitated by the addition of 60% perchloric acid to a final concentration of 0.5%. The soluble fraction containing ubiquitin was dialyzed overnight into 50 mM Na-acetate, pH 4.5, and purified by cation exchange on a 5 mL HiTrap SP FF column (GE) using a gradient of 0 - 0.5 M NaCl in 50 mM Na-acetate, pH 4.5. Peak fractions were concentrated and further purified over a Superdex S75 16/60 column in storage buffer (20 mM Tris-HCl, pH 7.6, 150 mM NaCl, 1 mM DTT). Ubiquitin was labeled by dialyzing into labeling buffer (30 mM HEPES, pH 7.2, 150 mM NaCl, 1 mM EDTA) and reacted with an excess of maleimide-fluorophore. The labeled ubiquitin was purified on a Superose 75 16/60 size exclusion column equilibrated in GF buffer, and its concentration was measured by the Lowry assay using non-labeled ubiquitin as a standard.

Purification of linear tetra-ubiquitin: A pET15b plasmid containing linearly fused tetra-ubiquitin with an N-terminal fusion to 6xHis-SUMO was generated by gene synthesis (Genscript). The plasmid was transformed into Rosetta2 (DE3) pLysS *E. coli*, grown in terrific broth at 37 °C until the OD_{600} = 0.6, and induced with 0.5 mM IPTG at 18 °C overnight. Cells were spun down and resuspended in NiA, lysed by sonication, and clarified by centrifugation. Lysate was purified on a HisTrap (GE) and eluted with NiA plus 250 mM imidazole. The His-SUMO tag was cleaved using SENP2 protease at 4 °C overnight, exchanged into 50 mM Na-acetate pH 4.5, syringe filtered through a 0.22 μm filter, purified by cation exchange on an SP FF column (GE) using a 0 - 500 mM NaCl gradient in 50 mM Na-acetate pH 4.5. Fractions containing tetra-ubiquitin were concentrated and purified by size-exclusion chromatography on a Superose 75 16/60 column equilibrated in GF buffer.

Purification of Rpn10: Purification of Rpn10 was conducted as previously described (Lander et al., 2012). Briefly, Bl21-star (DE3) E. coli cells were transformed with pACYCDuet-1 containing 6xHis-HRV-Rpn10. The cells were grown in dYT media at 37 °C until OD600 = 0.6-0.8. Protein expression was induced with 0.5 mM IPTG at 37 °C for 4 hr. After induction, the cells were harvested and resuspended in lysis buffer (60 mM HEPES, pH 7.6, 100 mM NaCl, 100 mM KCl, 20 mM Imidazole, 10% glycerol) containing 2 mg/mL lysozyme, benzonase, and protease inhibitors (aprotinin, pepstatin, leupeptin and PMSF). The cells were lysed by sonication, clarified by centrifugation, and the clarified lysate was bound in batch to 5 ml of Ni-NTA affinity resin (ThermoFisher). The resin was washed with lysis buffer and eluted with lysis buffer plus 250 mM imidazole. 2 mM DTT was added directly to the elution and the protein was cleaved overnight with HRV-protease. The next day the protein was purified using a Superdex 75 16/60 column equilibrated with lysis buffer.

Purification of Ubiquitination machinery: Mouse Uba1, yeast Ubc1, and yeast Rsp5 were all purified using the same procedure. Plasmids containing the gene were transformed into Rosetta2 (DE3) pLysS *E. coli* and grown in 6 L terrific broth at 37 °C. At an OD_{600} = 0.8, 1 mM IPTG was added to induce expression overnight at 18 °C. The cells were pelleted and resuspended in Buffer A (50 mM HEPES pH 7.6, 250 mM NaCl) with lysozyme, benzonase, pepstatin A, aprotinin and PMSF, and stored at −80 °C. The cells were thawed then lysed by sonication on ice. The lysate was spun down at 30,000 g for 30 min at 4 °C and the

supernatant was batch bound to HisPur Ni NTA resin (ThermoFisher) pre-equilibrated in Buffer A for one hour. The resin was poured into a column and washed with 50 mL Buffer A. The protein was eluted using Buffer A plus 250 mM imidazole. The protein was concentrated using an Amicon spin concentrator (Millipore) and then loaded onto a Superdex 200 16/60 column equilibrated in 20 mM HEPES 7.6, 100 mM NaCl and 10% glycerol. Mouse Uba1 was a gift from Jorge Eduardo Azevedo (Addgene plasmid # 32534) (Carvalho et al., 2012).

Purification of AMSH: The plasmid used to express AMSH, pOPINB-AMSH*, was a gift from David Komander (Addgene plasmid # 66712) and was purified as described previously (Michel et al., 2015). Plasmid containing the gene was transformed into Rosetta2 (DE3) pLysS *E. coli*, which were grown in 2 L of terrific broth to OD600 = 0.6. Protein expression was induced with 0.5 mM IPTG overnight at 18 °C, and then harvested in NiA buffer with lysozyme, benzonase and protease inhibitors. The cells were lysed by sonication, clarified by centrifugation at 30,000 g for 30 min and the protein was purified with a HisTrap. While bound to the HisTrap, the protein was washed with NiA buffer plus 10 mM ATP to remove contaminating DnaK. The 6xHis tag was removed by overnight incubation with HRV-protease and the protein was further purified by size-exclusion chromatography with a Superose 75 16/60 column equilibrated in GF.

Substrate ubiquitination: All substrates contained a PPPY motif in the unstructured region, which allows them to be ubiquitinated with long primarily K63-linked ubiquitin chains *in vitro* using the Rsp5 E3 ligase(Matyskiela et al., 2013; Saeki et al., 2005). Purified substrates (10 μM) were incubated for 3 hours at 25 °C in GF buffer with Uba1 (2.5 μM), Ubc1 (2.5 μM), Rsp5 (2.5 μM), ubiquitin (400 μM), and 10 mM ATP. Substrates were ubiquitinated fresh for each day of experiments and evaluated by gel to ensure reproducible ubiquitination.

Enzymatic Assays

Enzymatic assays: All enzymatic assays were performed at 25 °C in GF buffer supplemented with 5 mM ATP, 0.5 mM TCEP, 0.5 mg mL^{-1} BSA, and an ATP regeneration system (0.03 mg mL^{-1} creatine kinase and 16 mM creatine phosphate) unless otherwise noted.

All assays were performed with at least three technical replicates. The exact number of replicates (*N*) can be found in Tables S3–S8. Experiments in which substrate variants were compared were all performed on the same day using the same batches of purified enzymes. Occasionally, curves which were visually identified as large outliers were excluded from further analysis.

Anisotropy assays: Multiple-turnover degradations were monitored by tracking fluorescence anisotropy of fluorescein in a Synergy NEO2 multimode plate reader (Biotek). Reactions were initiated by mixing 6.5 μL of 2× reconstituted holoenzyme with 6.5 μL of 2× ubiquitinated substrate, then transferring 10 μL of the reaction to a 384-well flat bottom, low

volume microplate (Corning cat#3820). Final concentrations were 25 or 50 nM core, 400 nM base, 600 nM lid, 750 nM Rpn10, and varying concentrations of substrate.

Initial rates of processing were calculated by using the measured anisotropy of ubiquitinated substrate alone and that of substrate fully cleaved by chymotrypsin to normalize the measured change in anisotropy during the reaction.

To determine the Michaelis-Menten constants for titin-I27^{V15P}-23-K-1-FAM, the initial rate was normalized using substrate that had been fully deubiquitinated by Usp2 rather than fully degraded substrate. Because titin-I27^{V15P}-23-K-11-FAM and titin-I27^{V15P}-serine rich-FAM exhibit both degradation and deubiquitination, the chymotrypsin degraded value was used to normalize the curves, but the k_{cat} is not reported.

Final concentrations for all single-turnover degradations were 1.25 μM core, 2.5 μM base, 2.5 μM lid, 3 μM Rpn10, and 300 nM substrate. Single-turnover degradation measurements that were performed in a plate reader used a similar procedure as described above, with a deadtime of 8-10 seconds between mixing and the first measurement. Degradation measurements were also performed in an Auto SF120 stopped-flow fluorimeter (Kintek) with two photomultipliers to measure fluorescein anisotropy. The stopped-flow was loaded with 140 μL of 2× reconstituted holoenzyme and 140 μL of 2× substrate, with the same final concentrations as those used in the plate reader. After loading, four blank shots were fired, followed by three measurements. The deadtime of mixing on the instrument is sub-millisecond.

The curves for degradations measured in the stopped-flow and those measured in the plate reader were fit to a delayed exponential.

Gel Based Degradations: Single-turnover degradation measurements that were analyzed by gel were performed by mixing 2× reconstituted holoenzyme and 2× substrate, taking 2 μL aliquots at the indicated time, quenching them in 2% SDS-containing buffer, and separating the reaction by SDS-PAGE on 12% NuPAGE gels (Invitrogen) or 4-20% mini-protean TGX gels (Bio-rad). The fluorescence was then measured on a Typhoon FLA 9500 variable mode scanner (GE) using a pixel density of 50 μm per pixel.

Tail insertion assays: Tail insertion was measured by tracking Forster resonance energy transfer (FRET) between Cy3-labeled base and Cy5-labeled substrate, while enforcing single-turnover conditions using 1,10-phenanthroline (*o*PA), an inhibitor of Rpn11 that stalls the proteasome at the site of ubiquitin linkage (Worden et al., 2017). Base containing Rpt1^{I191AzF} was labeled with Sulfo-Cy3-DBCO (Click Chemistry Tools) as described above. A 30 mM *o*PA stock was made in GF buffer. Reactions were performed in the Auto SF120 using 2× reconstituted holoenzyme and 2× Sulfo-Cy3 labeled substrate. Final concentrations were 100 nM Cy3-Rpt1 base, 400 nM core, 600 nM lid, 750 nM Rpn10, 3 mM *o*PA, and 3 μM substrate. An excitation wavelength of 550 nm was used, and the Cy3 and Cy5 emission channels were monitored simultaneously.

The kinetics of tail insertion were determined by fitting the quenching of the Cy3 signal. The amplitudes listed in Table 1 were calculated by normalizing the amplitudes of the fast-

phases to the initial fluorescence, and then comparing those to the normalized amplitude of titin-I27^{V15P}-23-K-35-Cy5. All measurements used in this calculation were from traces collected on the same day.

Conformational change assays: The conformational state of the proteasome was monitored using FRET between Cy3-labeled lid and Cy5-labeled base. Lid containing Rpn9^{S111AzF} was labeled with Sulfo-Cy3-DBCO, and base containing Rpt5^{Q49AzF} was labeled with Sulfo-Cy5-DBCO as described above. Steady-state measurements were performed by mixing 2× reconstituted holoenzyme (150 nM Cy5-Rpt5 base, 400 nM core, 500 nM Cy3-Rpn9 lid, and 750 nM Rpn10) with 2× substrate or other additive as indicated. Final concentrations of the reconstituted holoenzyme were 150 nM Cy5-Rpt5 base, 400 nM core, 500 nM Cy3-Rpn9 lid, and 750 nM Rpn10. Final substrate concentration was 3 μM. Final *o*PA concentration was 3 mM. Catalytically dead Ubp6^{C188A} was added at 250 nM, and linear tetra-ubiquitin was added at 100 μM. ATPγS was added at 5 mM in place of the ATP regeneration system. The reactions were then transferred to a 384-well flat bottom, low volume microplate (Corning cat#3820), and the fluorescence intensities were measured in a Synergy NEO2 plate reader (Biotek). The steady-state levels of FRET were calculated by the following equation: $I_{a}cce_{p}t_{o}r/(I_{do}n_{o}r+Iacce_{p}t_{o}r)$. This value was calculated for each replicate and then averaged to determine the FRET signal for the respective condition. The FRET levels were then all normalized to that of the proteasome in ATP with no other additives.

Single turnover measurements were performed in the AutoSF 120 stopped-flow fluorimeter (Kintek) using 2× reconstituted holoenzyme with *o*PA (3 mM final) and 2× substrate, exciting at 550 nm and measuring Cy3 and Cy5 emission channels simultaneously. The kinetics of the conformational change were determined by fitting the gain of FRET observed in the Cy5 channel.

Deubiquitination assays: Deubiquitination was tracked using FRET between Cy3-labeled ubiquitin and a Cy5-labeled substrate. Sulfo-Cy3 labeled ubiquitin was used to ubiquitinate Sulfo-Cy5 labeled substrates in the same ubiquitination conditions as described above. Single-turnover degradation reactions were then performed as described above, but instead of tracking anisotropy, Cy3 was excited, and Cy3 and Cy5 emission were monitored. The kinetics of deubiquitination were determined by fitting the loss of FRET observed in the Cy5 channel.

Competition assays: The degradation competition experiments were performed similarly to the multiple-turnover degradation assays described above. The 2× reconstituted holoenzyme was mixed with a 2× solution containing both the labeled substrate and unlabeled competitor. The final concentrations of the experiment in Fig. 4D used were 50 nM core, 400 nM base, 600 nM lid, 750 nM Rpn10, 500 nM FAM-titin-I27^{V15P}-23-K-35, and varying competitor concentration. The experiment in Fig. S6C was performed with similar conditions, except the labeled substrates were at 2 DM final concentration and the concentration of titin-I27^{V15P}-23-K-35 was varied. The experiment in Fig. S1B was performed with the same proteasome component concentrations, but with 2 DM FAM-titin-

$I27^{V15P}$-23-K-35 and 100 DM linear tetra-ubiquitin where noted. The extent of inhibition was then calculated by comparison of the initial rates with and without the competitor.

Stability measurement: The equilibrium stability of titin mutants was measured by monitoring the tryptophan fluorescence of the substrate after equilibration at 25 °C with different concentrations of urea(Kenniston et al., 2003). The fluorescence (excitation = 280 nm, emission = 325 nm) was monitored in a plate reader at 25 °C. The curves were fit to the following system of equations: $y=(A+B*k)/(1+k)$; $A=A_0+m_A*[urea]$; $B=B_0+m_B*[urea]$; $k=e^{(-\Delta G/(RT)}$; $\Delta G= m*(c_m-[urea])$ All variables were fit globally across the three substrates, except for the c_m values. The ΔG_0 was then calculated using the equation $\Delta G_0= m*c_m$.

ATPase assays: The rate of ATP hydrolysis was measured using an NADH-coupled assay. Reconstituted proteasome (150 nM base, 400 nM core, 600 nM lid, 750 nM Rpn10, 1 mM ATP) was combined with ATPase mix (3 U ml^{-1} pyruvate kinase, 3 U ml^{-1} lactase dehydrogenase, 1 mM NADH, and 7.5 mM phosphoenolpyruvate), and the change of absorbance at 340 nm was monitored over time in a plate reader.

Ubiquitination state analysis: The number of ubiquitin chains on multi-lysine substrates was confirmed by both modification with methyl-ubiquitin and by treatment of wild-type ubiquitin modified substrates with the K63-specific deubiquitinase AMSH. Purified substrates (10 μM) were incubated for 3 hours at 25 °C in GF buffer with Uba1 (2.5 μM), Ubc1 (2.5 μM), Rsp5 (2.5 μM), 10 mM ATP, and varying ubiquitin. Methyl ubiquitinated substrates were modified with 120 μM methyl ubiquitin (Boston Biochem). For the AMSH treatment, substrates were modified with 400 μM wild-type ubiquitin, then treated with 20 μM AMSH for 30 minutes at RT before analysis by SDS-PAGE and visualization by 5-FAM fluorescence on a ChemiDoc (Bio-Rad). Because AMSH will only cleave K63-linked chains, it will not remove the proximal ubiquitin from the substrate.

Usp2 treated substrates are treated with 2 μM Usp2 for 30 minutes. Usp2 is a non-specific deubiquitinase, and will thus remove the proximal ubiquitin.

QUANTIFICATION AND STATISTICAL ANALYSIS

All curve fitting was done using Origin (Originlab, Northampton, MA) while plotting was done using Graphpad Prism. The fits were performed by least squares fitting, and visually evaluated by the distribution of the residuals to ensure there were no significant deviations from zero. For Michaelis Menten calculations, the initial rates from substrate degradation or deubiquitination experiments were fit to the Michaelis-Menten equation to determine kcat and KM. Exponential curves from single-turnover measurements were fit to either a double exponential increase/decay ($y=y_0 + A_1*e^{-t/\tau1} + A_2*e^{-t/\tau2}$) or a delayed double exponential increase/decay ($y=y_0 + A_1*e^{-(t-t0)/\tau1} + A_2*e^{-(t-t0)/\tau2}$), in which the delay was determined by visual inspection of the curves. In general, the fluorescence channel with the largest signal change was used for fitting and representative traces. Some curves were smoothened by the Savitsky-Golay method for visualization, but all data analysis was done on the raw traces. The plotted curves were normalized to the initial fluorescence value for each trace.

The slow phase of the double exponential fit was not used in the analyses, because it is thought to arise from a small population of partially aggregated or incompletely ubiquitinated substrate. In support of this, the fast phase of the single-turnover degradation kinetics match well with the kcat values measured in multiple turnover. The time constants for both phases and their relative distribution of amplitudes are reported in Tables S3–S8.

The stability measurements (Figure S3) were fit to the following system of equations: $y=(A+B*k)/(1+k)$; $A=A_0+m_A*[urea]$; $B=B_0+m_B*[urea]$; $k=e^{(-\Delta G(RT)}$; $AG= m*(c_m-[urea])$ All variables were fit globally across the three substrates, except for the cm values. The AG0 was then calculated using the equation $AG_0= m*c_m$.

The quantification in Figure 5 was done using Imagequant TL (GE), with each gel being internally normalized as noted before calculating the mean. All of the individual data points were used in the curve fitting of the ubiquitinated species. Because the titin-43-K-35 substrates gets degraded so quickly it was not possible to fit the data to a double exponential and thus a single exponential was used.

The number of technical replicates (*N*) and the relevant statistical parameters for each experiment (such as mean or s.d.) are described in the figure captions. Tables S3–S8 also report the mean and s.d. for all technical replicates performed. Occasionally, curves which were visually identified as large outliers were excluded from the analysis. No statistical methods were used to verify that the data met the assumptions of the statistical approach.

Supplementary Material

Refer to Web version on PubMed Central for supplementary material.

Acknowledgements:

We thank the members of the Martin lab for numerous helpful discussions. We also thank Ellen Goodall and Erika Lopez-Alfonso for providing some purified protein. Funding: J.A.M.B. and C.B. acknowledge support from NSF Graduate Research Fellowships. This research was funded in part by the US National Institutes of Health (R01-GM094497 to A.M.), the US National Science Foundation CAREER Program (NSF-MCB-1150288 to A.M.), and the Howard Hughes Medical Institute (K.C.D., and A.M.).

References:

Albert S, Schaffer M, Beck F, Mosalaganti S, Asano S, Thomas HF, Plitzko JM, Beck M, Baumeister W, and Engel BD (2017). Proteasomes tether to two distinct sites at the nuclear pore complex. Proc Natl Acad Sci U S A 114, 13726–13731. [PubMed: 29229809]

Amiram M, Haimovich AD, Fan C, Wang YS, Aerni HR, Ntai I, Moonan DW, Ma NJ, Rovner AJ, Hong SH, et al. (2015). Evolution of translation machinery in recoded bacteria enables multi-site incorporation of nonstandard amino acids. Nat Biotechnol 33, 1272–1279. [PubMed: 26571098]

Asano S, Fukuda Y, Beck F, Aufderheide A, Forster F, Danev R, and Baumeister W (2015). A molecular census of 26S proteasomes in intact neurons. Science 347, 439–442. [PubMed: 25613890]

Aufderheide A, Beck F, Stengel F, Hartwig M, Schweitzer A, Pfeifer G, Goldberg AL, Sakata E, Baumeister W, and Forster F (2015). Structural characterization of the interaction of Ubp6 with the 26S proteasome. PNAS 112, 8626–8631. [PubMed: 26130806]

Bard JAM, Goodall EA, Greene ER, Jonsson E, Dong KC, and Martin A (2018). Structure and Function of the 26S Proteasome. Annu Rev Biochem 87, 697–724. [PubMed: 29652515]

Bard JAM, and Martin A (2018). Recombinant Expression, Unnatural Amino Acid Incorporation, and Site-Specific Labeling of 26S Proteasomal Subcomplexes. Methods Mol Biol 1844, 219–236. [PubMed: 30242713]

Bashore C, Dambacher CM, Goodall EA, Matyskiela ME, Lander GC, and Martin A (2015). Ubp6 deubiquitinase controls conformational dynamics and substrate degradation of the 26S proteasome. Nature structural & molecular biology 22, 712–719.

Bauerlein FJB, Saha I, Mishra A, Kalemanov M, Martinez-Sanchez A, Klein R, Dudanova I, Hipp MS, Hartl FU, Baumeister W, et al. (2017). In Situ Architecture and Cellular Interactions of PolyQ Inclusions. Cell 171, 179–187 e110. [PubMed: 28890085]

Beck F, Unverdorben P, Bohn S, Schweitzer A, Pfeifer G, Sakata E, Nickell S, Plitzko JM, Villa E, Baumeister W, et al. (2012). Near-atomic resolution structural model of the yeast 26S proteasome. Proc Natl Acad Sci USA 109, 14870–14875. [PubMed: 22927375]

Beckwith R, Estrin E, Worden EJ, and Martin A (2013). Reconstitution of the 26S proteasome reveals functional asymmetries in its AAA+ unfoldase. Nat Struct Mol Biol 20, 1164–1172. [PubMed: 24013205]

Bhattacharyya S, Renn JP, Yu H, Marko JF, and Matouschek A (2016). An assay for 26S proteasome activity based on fluorescence anisotropy measurements of dye-labeled protein substrates. Analytical biochemistry 509, 50–59. [PubMed: 27296635]

Blythe EE, Olson KC, Chau V, and Deshaies RJ (2017). Ubiquitin- and ATP-dependent unfoldase activity of P97/VCP*NPLOC4*UFD1L is enhanced by a mutation that causes multisystem proteinopathy. Proc Natl Acad Sci U S A 114, E4380–E4388. [PubMed: 28512218]

Bodnar NO, and Rapoport TA (2017). Molecular Mechanism of Substrate Processing by the Cdc48 ATPase Complex. Cell 169, 722–735 e729. [PubMed: 28475898]

Carvalho AF, Pinto MP, Grou CP, Vitorino R, Domingues P, Yamao F, Sa-Miranda C, and Azevedo JE (2012). High-yield expression in Escherichia coli and purification of mouse ubiquitin-activating enzyme E1. Molecular biotechnology 51, 254–261. [PubMed: 22012022]

Chatterjee A, Sun SB, Furman JL, Xiao H, and Schultz PG (2013). A versatile platform for single- and multiple-unnatural amino acid mutagenesis in Escherichia coli. Biochemistry 52, 1828–1837. [PubMed: 23379331]

Chen B, Retzlaff M, Roos T, and Frydman J (2011). Cellular strategies of protein quality control. Cold Spring Harb Perspect Biol 3, a004374. [PubMed: 21746797]

Chin JW, Santoro SW, Martin AB, King DS, Wang L, and Schultz PG (2002). Addition of p-azido-L-phenylalanine to the genetic code of Escherichia coli. J Am Chem Soc 124, 9026–9027. [PubMed: 12148987]

Crosas B, Hanna J, Kirkpatrick DS, Zhang DP, Tone Y, Hathaway Nathaniel A., Buecker C, Leggett DS, Schmidt M, King RW, et al. (2006). Ubiquitin Chains Are Remodeled at the Proteasome by Opposing Ubiquitin Ligase and Deubiquitinating Activities. Cell 127, 1401–1413. [PubMed: 17190603]

de la Pena AH, Goodall EA, Gates SN, Lander GC, and Martin A (2018). Substrate-engaged 26S proteasome structures reveal mechanisms for ATP-hydrolysis-driven translocation. Science 362.

Deveraux Q, Ustrell V, Pickart C, and Rechsteiner M (1994). A 26 S protease subunit that binds ubiquitin conjugates. J Biol Chem 269, 7059–7061. [PubMed: 8125911]

Dong Y, Zhang S, Wu Z, Li X, Wang WL, Zhu Y, Stoilova-McPhie S, Lu Y, Finley D, and Mao Y (2018). Cryo-EM structures and dynamics of substrate-engaged human 26S proteasome. Nature.

Elsasser S, Chandler-Militello D, Muller B, Hanna J, and Finley D (2004). Rad23 and Rpn10 serve as alternative ubiquitin receptors for the proteasome. J Biol Chem 279, 26817–26822. [PubMed: 15117949]

Erales J, Hoyt MA, Troll F, and Coffino P (2012). Functional asymmetries of proteasome translocase pore. J Biol Chem 287, 18535–18543. [PubMed: 22493437]

Fishbain S, Inobe T, Israeli E, Chavali S, Yu H, Kago G, Babu MM, and Matouschek A (2015). Sequence composition of disordered regions fine-tunes protein half-life. Nature Structural & Molecular Biology 22, 214–221.

Fishbain S, Prakash S, Herrig A, Elsasser S, and Matouschek A (2011). Rad23 escapes degradation because it lacks a proteasome initiation region. Nature communications 2, 192.

Glickman MH, Rubin DM, Fried VA, and Finley D (1998). The regulatory particle of the Saccharomyces cerevisiae proteasome. Molecular and cellular biology 18, 3149–3162. [PubMed: 9584156]

Groll M, Bajorek M, Kohler A, Moroder L, Rubin DM, Huber R, Glickman MH, and Finley D (2000). A gated channel into the proteasome core particle. Nat Struct Biol 7, 1062–1067. [PubMed: 11062564]

Guo Q, Lehmer C, Martinez-Sanchez A, Rudack T, Beck F, Hartmann H, Perez-Berlanga M, Frottin F, Hipp MS, Hartl FU, et al. (2018). In Situ Structure of Neuronal C9orf72 Poly-GA Aggregates Reveals Proteasome Recruitment. Cell 172, 696–705 e612. [PubMed: 29398115]

Hershko A, and Ciechanover A (1998). The ubiquitin system. Annu Rev Biochem 67, 425–479. [PubMed: 9759494]

Hu M, Li P, Song L, Jeffrey PD, Chenova TA, Wilkinson KD, Cohen RE, and Shi Y (2005). Structure and mechanisms of the proteasome-associated deubiquitinating enzyme USP14. The EMBO Journal 24, 3747–3756. [PubMed: 16211010]

Husnjak K, Elsasser S, Zhang N, Chen X, Randles L, Shi Y, Hofmann K, Walters KJ, Finley D, and Dikic I (2008). Proteasome subunit Rpn13 is a novel ubiquitin receptor. Nature 453, 481–488. [PubMed: 18497817]

Inobe T, Fishbain S, Prakash S, and Matouschek A (2011). Defining the geometry of the two-component proteasome degron. Nat Chem Biol 7, 161–167. [PubMed: 21278740]

Johnston JA, Johnson ES, Waller PR, and Varshavsky A (1995). Methotrexate inhibits proteolysis of dihydrofolate reductase by the N-end rule pathway. J Biol Chem 270, 8172–8178. [PubMed: 7713922]

Kenniston JA, Baker TA, Fernandez JM, and Sauer RT (2003). Linkage between ATP consumption and mechanical unfolding during the protein processing reactions of an AAA+ degradation machine. Cell 114, 511–520. [PubMed: 12941278]

Kirkpatrick DS, Hathaway NA, Hanna J, Elsasser S, Rush J, Finley D, King RW, and Gygi SP (2006). Quantitative analysis of in vitro ubiquitinated cyclin B1 reveals complex chain topology. Nature cell biology 8, 700–710. [PubMed: 16799550]

Kraut DA, Israeli E, Schrader EK, Patil A, Nakai K, Nanavati D, Inobe T, and Matouschek A (2012). Sequence- and species-dependence of proteasomal processivity. ACS chemical biology 7, 1444–1453. [PubMed: 22716912]

Lander GC, Estrin E, Matyskiela ME, Bashore C, Nogales E, and Martin A (2012). Complete subunit architecture of the proteasome regulatory particle. Nature 482, 186–191. [PubMed: 22237024]

Lu Y, Lee BH, King RW, Finley D, and Kirschner MW (2015). Substrate degradation by the proteasome: a single-molecule kinetic analysis. Science 348, 1250834. [PubMed: 25859050]

Matyskiela ME, Lander GC, and Martin A (2013). Conformational switching of the 26S proteasome enables substrate degradation. Nat Struct Mol Biol 20, 781–788. [PubMed: 23770819]

Michel MA, Elliott PR, Swatek KN, Simicek M, Pruneda JN, Wagstaff JL, Freund SMV, and Komander D (2015). Assembly and Specific Recognition of K29-and K33-Linked Polyubiquitin. Molecular Cell 58, 95–109. [PubMed: 25752577]

Mikolajczyk J, Drag M, Bekes M, Cao JT, Ronai Z, and Salvesen GS (2007). Small ubiquitin-related modifier (SUMO)-specific proteases - Profiling the specificities and activities of human SENPs. Journal of Biological Chemistry 282, 26217–26224. [PubMed: 17591783]

Olszewski MM, Williams C, Dong KC, and Martin A (2019). The Cdc48 unfoldase prepares well-folded protein substrates for degradation by the 26S proteasome. Communications Biology 2, 29. [PubMed: 30675527]

Pathare GR, Nagy I, Sledz P, Anderson DJ, Zhou HJ, Pardon E, Steyaert J, Forster F, Bracher A, and Baumeister W (2014). Crystal structure of the proteasomal deubiquitylation module Rpn8-Rpn11. Proc Natl Acad Sci U S A 111, 2984–2989. [PubMed: 24516147]

Peth A, Nathan JA, and Goldberg AL (2013). The ATP costs and time required to degrade ubiquitinated proteins by the 26 s proteasome. J Biol Chem 288, 29215–29222. [PubMed: 23965995]

Peth A, Uchiki T, and Goldberg AL (2010). ATP-dependent steps in the binding of ubiquitin conjugates to the 26S proteasome that commit to degradation. Mol Cell 40, 671–681. [PubMed: 21095592]

Prakash S, Tian L, Ratliff KS, Lehotzky RE, and Matouschek A (2004). An unstructured initiation site is required for efficient proteasome-mediated degradation. Nat Struct Mol Biol 11, 830–837. [PubMed: 15311270]

Rape M, Reddy SK, and Kirschner MW (2006). The processivity of multiubiquitination by the APC determines the order of substrate degradation. Cell 124, 89–103. [PubMed: 16413484]

Rodnina MV, and Wintermeyer W (2001). Ribosome fidelity: tRNA discrimination, proofreading and induced fit. Trends Biochem Sci 26, 124–130. [PubMed: 11166571]

Saeki Y, Isono E, and Toh EA (2005). Preparation of ubiquitinated substrates by the PY motif-insertion method for monitoring 26S proteasome activity. Methods in enzymology 399, 215–227. [PubMed: 16338358]

Shabek N, Herman-Bachinsky Y, Buchsbaum S, Lewinson O, Haj-Yahya M, Hejjaoui M, Lashuel HA, Sommer T, Brik A, and Ciechanover A (2012). The size of the proteasomal substrate determines whether its degradation will be mediated by mono- or polyubiquitylation. Mol Cell 48, 87–97. [PubMed: 22902562]

Shi Y, Chen X, Elsasser S, Stocks BB, Tian G, Lee B-H, Shi Y, Zhang N, Poot SAH, Tuebing F, et al. (2016). Rpn1 provides adjacent receptor sites for substrate binding and deubiquitination by the proteasome. Science 351, aad9421. [PubMed: 26912900]

Sledz P, Unverdorben P, Beck F, Pfeifer G, Schweitzer A, Forster F, and Baumeister W (2013). Structure of the 26S proteasome ath ATP-yS bound provides insights into the mechanism of nucleotide-dependent substrate translocation. Proc Natl Acad Sci U S A 110, 7264–7269. [PubMed: 23589842]

Takeuchi J, Chen H, and Coffino P (2007). Proteasome substrate degradation requires association plus extended peptide. The EMBO Journal 26, 123–131. [PubMed: 17170706]

Theile CS, Witte MD, Blom AEM, Kundrat L, Ploegh HL, and Guimaraes CP (2013). Site-specific N-terminal labeling of proteins using sortase-mediated reactions. Nature protocols 8, 1800–1807. [PubMed: 23989674]

Unverdorben P, Beck F, Sledz P, Schweitzer A, Pfeifer G, Plitzko JM, Baumeister W, and Forster F (2014). Deep classification of a large cryo-EM dataset defines the conformational landscape of the 26S proteasome. Proc Natl Acad Sci U S A 111, 5544–5549. [PubMed: 24706844]

van Geel R, Pruijn GJ, van Delft FL, and Boelens WC (2012). Preventing thiol-yne addition improves the specificity of strain-promoted azide-alkyne cycloaddition. Bioconjugate chemistry 23, 392–398. [PubMed: 22372991]

van Nocker S, Sadis S, Rubin DM, Glickman M, Fu H, Coux O, Wefes I, Finley D, and Vierstra RD (1996). The multiubiquitin-chain-binding protein Mcb1 is a component of the 26S proteasome in Saccharomyces cerevisiae and plays a nonessential, substrate-specific role in protein turnover. Molecular and cellular biology 16, 6020–6028. [PubMed: 8887631]

Verma R, Aravind L, Oania R, McDonald WH, Yates JR 3rd, Koonin EV, and Deshaies RJ (2002). Role of Rpn11 metalloprotease in deubiquitination and degradation by the 26S proteasome. Science 298, 611–615. [PubMed: 12183636]

Wehmer M, Rudack T, Beck F, Aufderheide A, Pfeifer G, Plitzko JM, Forster F, Schulten K, Baumeister W, and Sakata E (2017). Structural insights into the functional cycle of the ATPase module of the 26S proteasome. Proc Natl Acad Sci U S A 114, 1305–1310. [PubMed: 28115689]

Worden EJ, Dong KC, and Martin A (2017). An AAA Motor-Driven Mechanical Switch in Rpn11 Controls Deubiquitination at the 26S Proteasome. Mol Cell 67, 799–811 .e798. [PubMed: 28844860]

Worden EJ, Padovani C, and Martin A (2014). Structure of the Rpn11-Rpn8 dimer reveals mechanisms of substrate deubiquitination during proteasomal degradation. Nature Structural & Molecular Biology 21, 220–227.

Yao T, and Cohen RE (2002). A cryptic protease couples deubiquitination and degradation by the proteasome. Nature 419, 403–407. [PubMed: 12353037]

Yu H, Singh Gautam AK, Wilmington SR, Wylie D, Martinez-Fonts K, Kago G, Warburton M, Chavali S, Inobe T, Finkelstein IJ, et al. (2016). Conserved Sequence Preferences Contribute to Substrate Recognition by the Proteasome. J Biol Chem.

Highlights

- The rate-limiting step of protein degradation by the proteasome is unfolding.
- Substrate contact with the motor triggers a conformational switch of the proteasome.
- Substrates with poor initiation regions are quickly rejected.
- Supernumerary ubiquitin chains promote degradation of otherwise poor substrates.

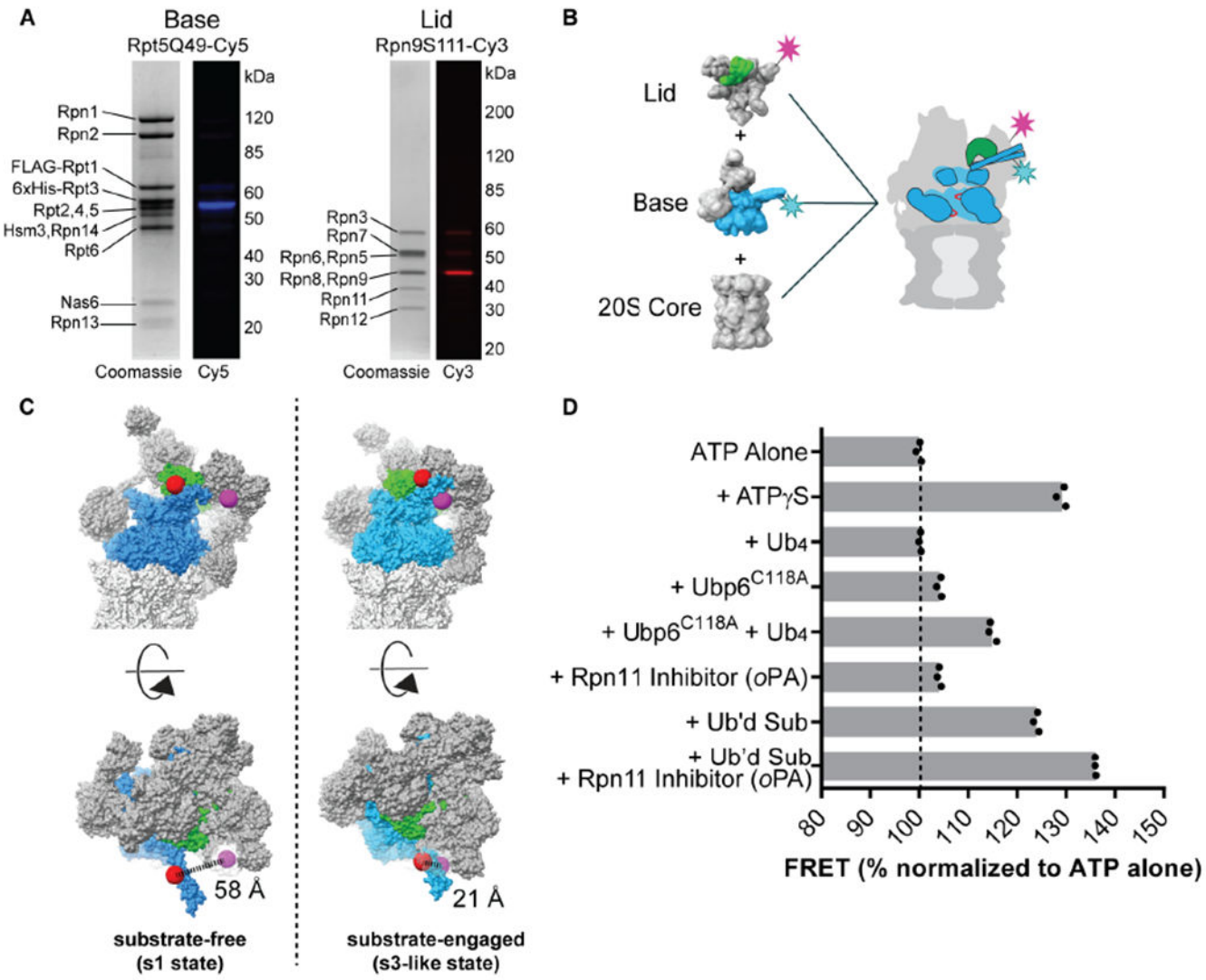

Figure 1. Site-specific labeling of the 26S proteasome and a steady-state assay for its conformations.

(**A**) SDS-PAGE analysis of base and lid with AzF incorporated into Rpt5 and Rpn9, and then labeled with Cy5 and Cy3, respectively. (**B**) Schematic for the *in vitro* reconstitution of the 26S proteasome. (**C**) Comparison of the substrate-free and substrate-engaged states. The distance between Rpt5-Q49 and Rpn9-S111 changes by 37 Å during the conformational transition. The AAA+ ATPases are blue, Rpn11 is green, and the rest of the regulatory particle as well as the 20S core are grey. Models were generated from surface representations of atomic models (PDB: 5mp9, 5mpd, 5mpb). The red and purple spheres indicate the labeled residues in Rpt5 and Rpn9, respectively.

(**D**) Steady-state FRET between Cy3-labeled lid (RpnS111AzF-Cy3) and Cy5-labeled base (Rpt5Q49AzF-Cy5) under various conditions, normalized to the signal for proteasome with ATP alone. $Ubp6^{C118A}$ is catalytically inactive, Ub_4 represents a linearly fused tetra-ubiquitin, and the ubiquitinated substrate is titin-$I27^{V15P}$-23-K-35. Shown are the mean and individual measurements for $N = 3$. See also Figure S1.

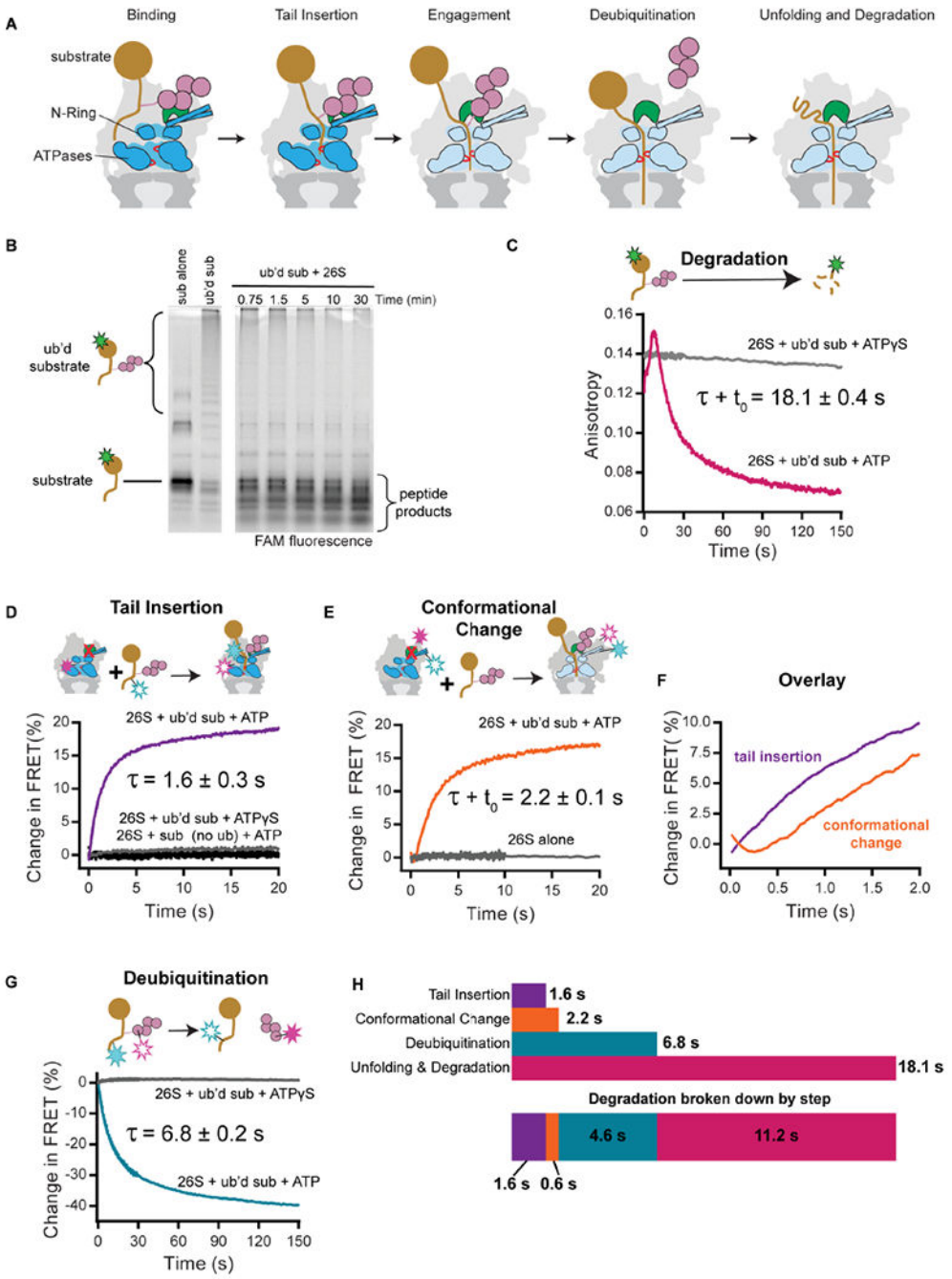

Figure 2. Substrate engagement triggers the conformational switch of the proteasome.

(**A**) Schematic for the substrate processing pathway. Ubiquitin chains (pink) target a substrate (gold) to the 26S proteasome in the s1 state. The substrate's unstructured tail is inserted into the pore of the AAA+ motor (blue), where it interacts with pore loops (red) that drive translocation. After substrate engagement, the regulatory particle changes its conformation to an s3-like state and Rpn11 (green) shifts to a central position that allows translocation-coupled deubiquitination. Ubiquitin-chain removal is followed by mechanical substrate unfolding and threading of the polypeptide into the 20S core for proteolytic

cleavage. (**B**) Single-turnover degradation of ubiquitinated 5-FAM-titin-I27^{V15P}-23-K-35 by reconstituted 26S proteasome is tracked by SDS-PAGE and visualized by 5-FAM fluorescence. (**C**) Single-turnover degradation of ubiquitinated 5-FAM-titin-I27^{V15P}-23-K-35 is tracked by fluorescence anisotropy in the presence of ATP or ATP**γ**S. The total time for degradation is derived from the sum of the time constant **τ** for the exponential decay of anisotropy and the time t_0 for the initial anisotropy increase. (**D**) Substrate-tail insertion is tracked by FRET between the 26S proteasome reconstituted with Cy3-labeled base (Rpt1-I191AzF-Cy3) and ubiquitinated titin-I27^{V15P}-23-K-35 modified with Cy5 on its unstructured tail. At t=0, an excess of substrate was added to proteasomes with *o*PA-inhibited Rpn11 in the presence of either ATP (purple) or ATP**γ**S (grey). A control with non-ubiquitinated, Cy3-labeled titin-I27^{V15P}-23-K-35 substrate is depicted in black. Shown is the signal of the Cy3 channel, normalized to initial fluorescence. (**E**) Conformational state of the proteasome over time, tracked by FRET between Cy5-labeled base (Rpt5Q49AzF-Cy5) and Cy3-labled lid (Rpn9S111AzF-Cy3). At t=0, an excess of ubiquitinated titin-I27^{V15P}-23-K-35 or buffer was added to double-labeled proteasomes with *o*PA-inhibited Rpn11. Shown is the Cy5 channel, normalized to initial fluorescence. The total time for the conformational change is derived from the sum of the time constant **τ** for the exponential increase of FRET and the time t_0 for the initial delay. (**F**) Overlay of fluorescence traces for tail insertion and conformational change from **D** and **E** reveal a delay of 400 ms. (**G**) Deubiquitination tracked by FRET between Cy3-labeled ubiquitin and a Cy5 label attached adjacent to the single ubiquitinated lysine in titin-I27^{V15P}-23-K-35. At t=0 the substrate was mixed with excess proteasome in the presence of ATP or ATP**γ**S. Shown is the Cy5 channel, normalized to initial fluorescence. (**H**) Time constants of the substrate-processing steps as calculated from each assay individually or after accounting for the preceding steps. All curves in **C** – **G** are representative traces, and time constants are derived from averaging fits of independent experiments, shown with s.d. ($N \geq 3$). See also Figure S1 and S2.

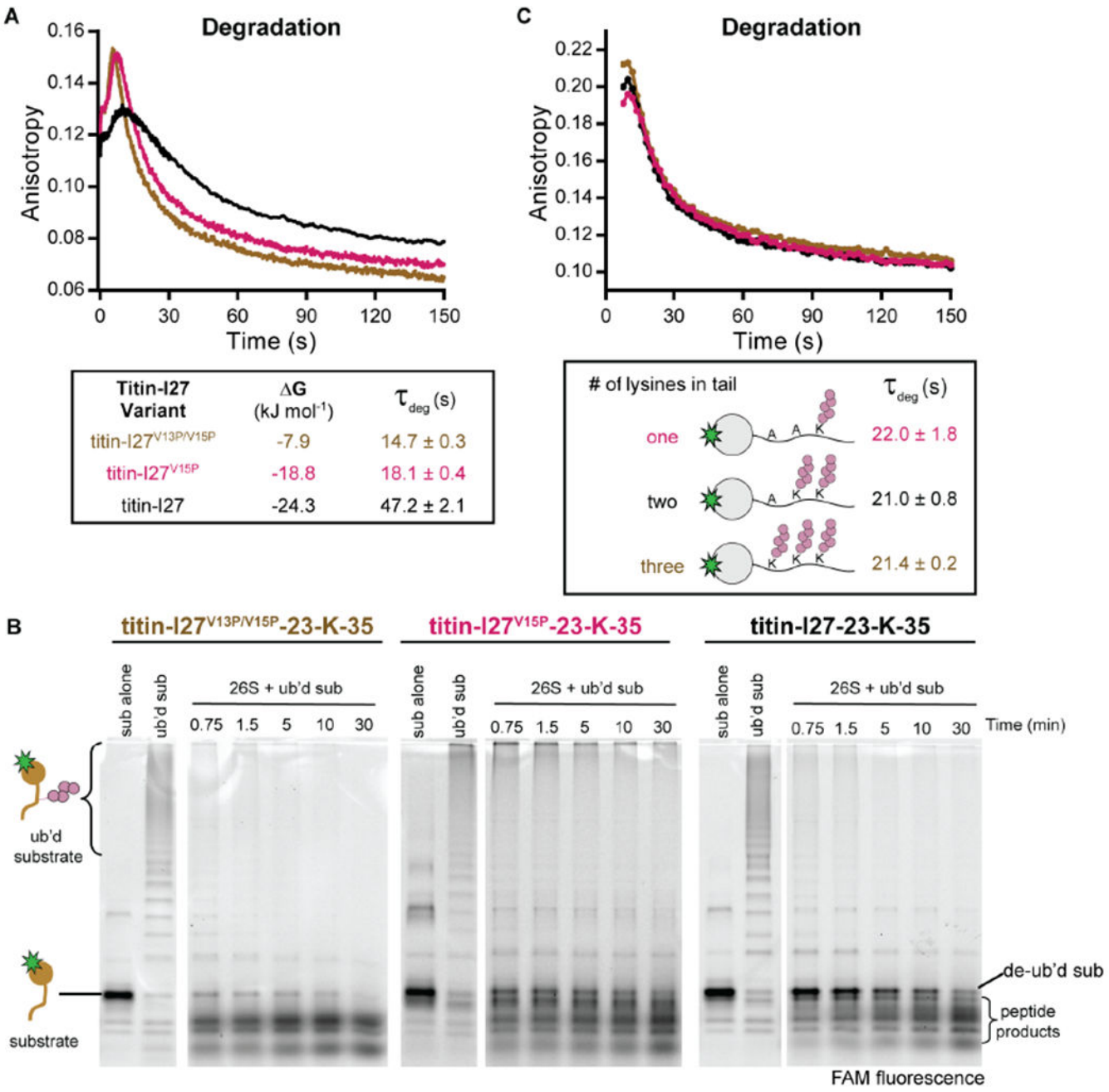

Figure 3. Increasing substrate stability slows degradation, but multiple ubiquitin chains can be rapidly removed.

(**A**) Single-turnover degradations of substrates with mutations in the titin-I27 folded domain tracked by anisotropy of N-terminally attached 5-FAM. Stabilities were determined by denaturant-induced equilibrium unfolding (see Fig. S3). (**B**) Singleturnover degradations of the same substrates as in **A**, but tracked by SDS-PAGE. (**C**) Single-turnover degradations of substrates with up to 3 lysine-attached ubiquitin chains in the unstructured tail tracked by anisotropy of 5-FAM. All curves are representative traces, and time constants are derived

from averaging fits of independent experiments, shown with s.d. ($N \geq 3$). See also Figure S3 and S4.

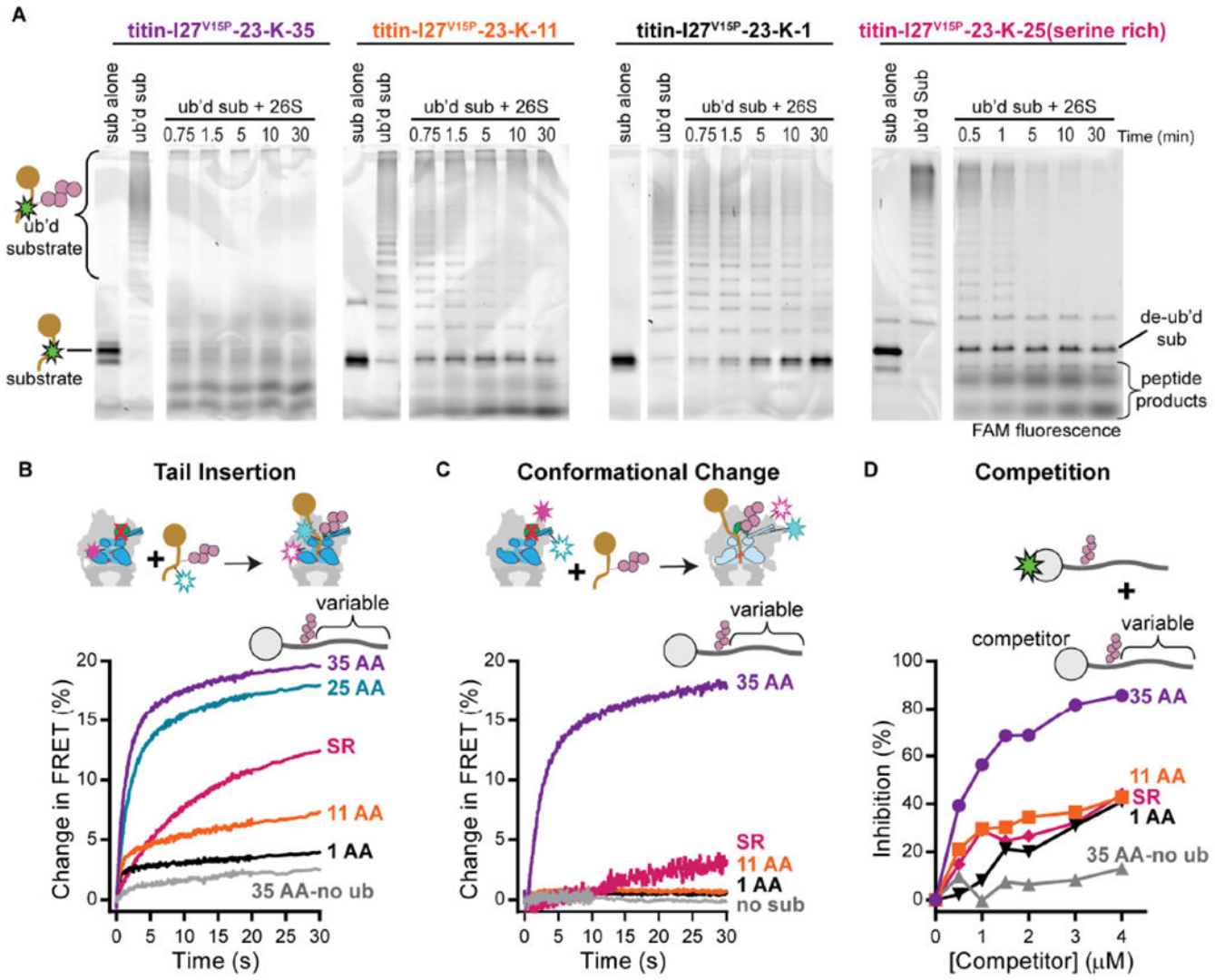

Figure 4. Substrates with poor initiation regions do not stably engage with the proteasome.

(**A**) Single-turnover degradations of substrates with varied unstructured initiation regions analyzed by SDS-PAGE. (**B**) Tail insertion kinetics of substrate variants tracked by FRET between the substrate and the proteasome as in Fig. 2D. The corresponding time constants are listed in Table 1. (**C**) Conformational change of the proteasome after substrate addition, tracked by FRET between the base and the lid as in Fig. 2E. (**D**) Competitive inhibition of titin-I27^{V15P}-23-K-35 degradation by substrates with varied tails (same substrates as in **C**). The percent inhibition is derived from the initial degradation rates in the presence and absence of competitor. All curves are representative traces ($N \geq 3$). See also Figure S5 and S6.

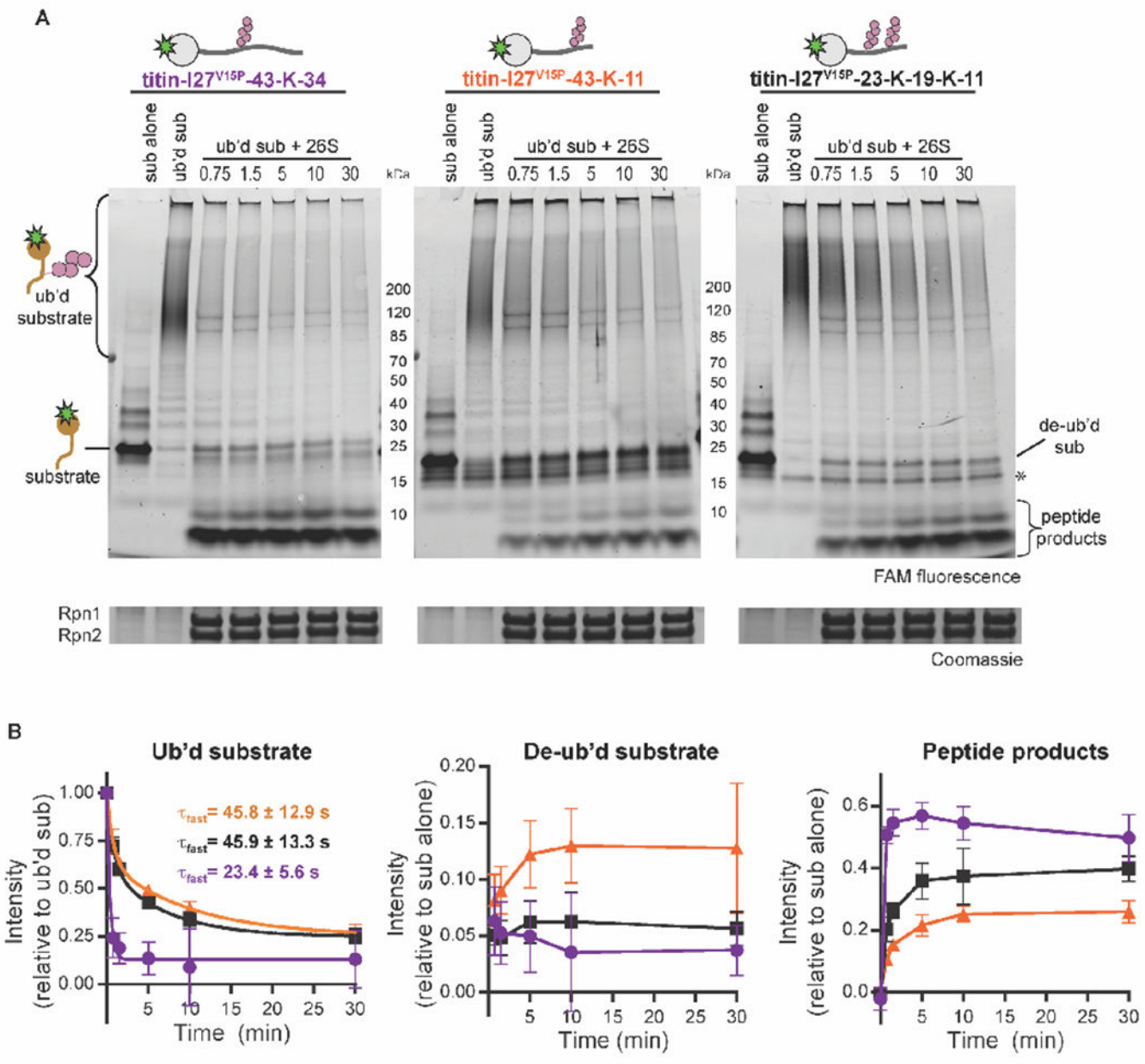

Figure 5. An extra ubiquitin chain promotes complete degradation of a substrate with a ubiquitin-obstructed initiation region.

(**A**) Single-turnover processing of substrates with varied unstructured initiation regions and ubiquitination states analyzed by SDS-PAGE. The substrate alone sample was generated by incubation of ubiquitinated substrate with Usp2. Coomassie-stained Rpn1 and Rpn2 are shown as a loading control. (**B**) Quantification of the fluorescence intensities shown in (A). The intensities for ubiquitinated substrate during proteasomal processing are normalized to the intensities for ubiquitinated substrate alone, while the intensities for deubiquitinated substrate and peptide product are normalized to the Usp2-treated samples (shown with means and s.d., $N \geq 3$). The curves for the ubiquitinated substrate panel are taken from exponential fits (see Table S8).

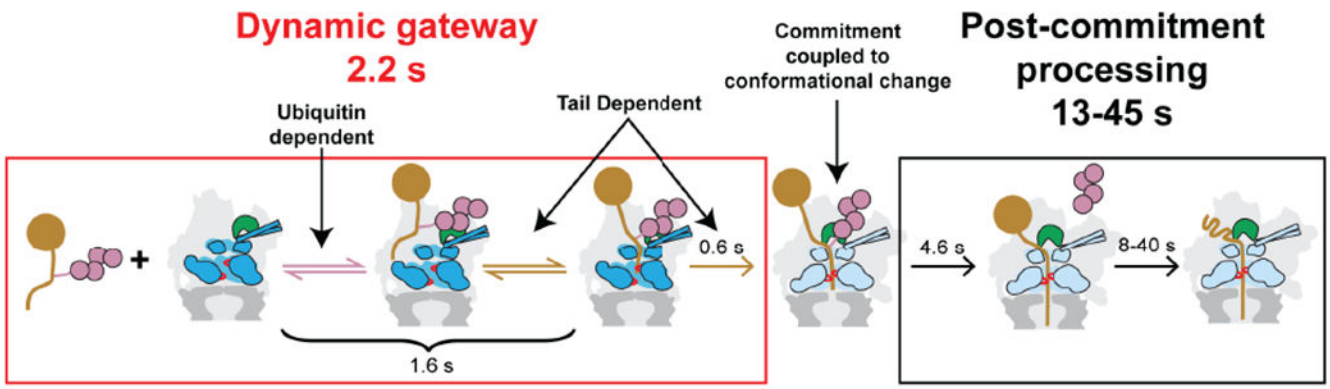

Figure 6. Model for kinetic proofreading by the proteasome.

Ubiquitin binding and tail insertion constitute a dynamic gateway to proteasomal substrate processing, with both fast on and off rates. If the substrate has the necessary requirements for degradation, engagement with the AAA+ motor reduces k_{off} for tail insertion and accelerates the conformational switch of the proteasome, thereby committing substrates to translocation-coupled deubiquitination, rate-limiting unfolding, and degradation.

Table 1:

Fast phase kinetics and amplitudes of substrate tail insertion as seen in Fig. 4B. Shown are the mean and s.d.. See also Table S4.

Substrate	τapp (s)	k_{app} ($1/\tau_{app}$, s^{-1})	Amplitude (Normalized to 35 AA tail)
titin-I27^{V15P}-23-K-35 (*N* = 9)	1.61 ± 0.32	0.62 ± 0.12	1 ± 0.03
titin-I27^{V15P}-23-K-25 (serine rich) (*N* = 5)	7.15 ± 1.00	0.14 ± 0.02	0.51 ± 0.04
titin-I27^{V15P}-23-K-25 (*N* = 3)	1.73 ± 0.02	0.58 ± 0.007	0.87 ± 0.05
titin-I27^{V15P}-23-K-11 (*N* = 3)	0.7 ± 0.09	1.4 ± 0.18	0.24 ± 0.01
titin-I27^{V15P}-23-K-1 (*N* = 3)	0.46 ± 0.03	2.2 ± 0.14	0.16 ± 0.001

KEY RESOURCES TABLE

REAGENT or RESOURCE	SOURCE	IDENTIFIER
Bacterial and Virus Strains		
Escherichia coli Rosetta2 (DE3) pLysS	Novagen	Cat#71403–3
Escherichia coli Bl21-star (DE3)	Thermofisher	Cat#C601003
Chemicals, Peptides, and Recombinant Proteins		
5-FAM-HHHHHHLPETGG	Biomatik	N/A
5-FAM-LPETGG	Genscript	N/A
Cy3 DBCO	Click Chemistry Tools	Cat#A140
Cy3 Maleimide	Click Chemistry Tools	Cat#1009
Cy5 DBCO	Click Chemistry Tools	Cat#A130
Cy5 Maleimide	Click Chemistry Tools	Cat#1004
4-azido-L-phenylalanine	Amatek Chemical	Cat#A-7137
1,10-phenanthroline	Sigma	Cat#P9375
5-FAM maleimide	Thermo	Cat#62245
Methylated ubiquitin	Boston Biochem	Cat#U-501
Experimental Models: Organisms/Strains		
Saccharomyces Cerevisiae yAM54 with Pre1-3xFLAG	(Beckwith et al., 2013)	N/A
Recombinant DNA		
Usp2	Cheryl Arrowsmith	Addgene 36894
SENP2	Guy Salvesen (Mikolajczyk et al., 2007)	Addgene 16357
AMSH	David Komander (Michel et al., 2015)	Addgene 66712
Mouse E1	Jorge Eduardo Azevedo (Carvalho et al., 2012)	Addgene 32534
Rpn10	(Lander et al., 2012)	N/A
Ubiquitin	(Worden et al., 2014)	N/A
Rsp5	(Worden et al., 2017)	N/A
Ubc1	(Lander et al., 2012)	N/A
$Ubp6^{C188A}$	(Bashore et al., 2015)	N/A

pAM81 Rpn1, Rpn1, Rpn13	(Beckwith et al., 2013)	N/A
pAM82 3xFLAG-Rpt1, Rpt2, 6xHis-Rpt3, Rpt4, Rpt5, Rpt6	(Beckwith et al., 2013)	N/A
pAM83 Nas2, Nas6, Hsm3, Rpn14, rare tRNAs	(Beckwith et al., 2013)	N/A
pAM87 AzFRS.2.t1, UAG-tRNA	This study	N/A
pAM88 3xFLAG-Rpt1I191TAG, Rpt2, 6xHis-Rpt3, Rpt4, Rpt5, Rpt6	This study	N/A
pAM89 3xFLAG-Rpt1, Rpt2, 6xHis-Rpt3, Rpt4, Rpt5Q49TAG, Rpt6	This study	N/A
pAM80 Sem1, Hsp90	This study	N/A
pAM85 Rpn5, MBP-HRV-Rpn6, Rpn8, Rpn9, Rpn11	This study	N/A
pAM86 Rpn3, Rpn7, 6xHis-HRV-Rpn12	This study	N/A
pAM90 Rpn5, MBP-HRV-Rpn6, Rpn8, Rpn9S111TAG, Rpn11	This study	N/A
pAM91 GGG-titin-I27V15P-23-K-9-C-25-intein-CBD	This study	N/A
pAM92 GGG-titin-I27V15P-21-C-2-K-35-intein-CBD	This study	N/A
pAM93 GGG-titin-I27-23-K-9-C-25-intein-CBD	This study	N/A
pAM94 GGG-titin-I27V13P/V15P-23-K-9-C-25-intein-CBD	This study	N/A
pAM95 GGG-titin-I27V15P-43-K-8-C-25-intein-CBD	This study	N/A
pAM96 GGG-titin-I27V15P-33-K-9-K-8-C-25	This study	N/A
pAM97 GGG-titin-I27V15P-23-K-9-K-9-K-8-C-25	This study	N/A
pAM98 titin-I27V15P-23-K-9-C-15	This study	N/A
pAM99 titin-I27V15P-23-K-9-C-1	This study	N/A
pAM100 titin-I27V15P-21-C-2-K-1	This study	N/A
pAM101 titin-I27V15P-23-K-9-C-15 serine rich	This study	N/A
pAM102 6xHis-Sumo-Ub-Ub-Ub-Ub	This study	N/A
pAM103 MC-Ubiquitin	This study	N/A
pAM104 titin-I27V15P-43-K-11	This study	N/A
pAM105 titin-I27V15P-23-K-19-K-11	This study	N/A
Software and Algorithms		
Origin Pro	OriginLab	http://www.originlab.com/
Imagequant TL	GE	https://www.gelifesciences.com/en/us/shop/protein-analysis/molecular-imaging-for-proteins/imaging-software/imagequant-tl-8-1-p-00110
Prism	Graphpad	https://www.graphpad.com/scientific-software/prism/

Other		
AutoSF-120 stopped flow fluorimeter	Kintek	N/A
Synergy Neo2 plate reader	Biotek	N/A
ChemiDoc MP	Bio-Rad	N/A